Discovery of Novel Naphthylphenylketone and Naphthylphenylamine Derivatives as Cell Division Cycle 25B (CDC25B) Phosphatase Inhibitors: Design, Synthesis, Inhibition Mechanism and *in Vitro* Efficacy against Melanoma Cell Lines

Carmen Cerchia,[1,+] Rosarita Nasso,[2,4,+] Matteo Mori,[3+] Stefania Villa,[3] Arianna Gelain[3], Alessandra Capasso,[2] Federica Aliotta,[2] Martina Simonetti,[2] Rosario Rullo,[2,5] Mariorosario Masullo,[4] Emmanuele De Vendittis,[2] Maria Rosaria Ruocco,[2,*] Antonio Lavecchia[1,*]

[1] *Department of Pharmacy, "Drug Discovery" Laboratory, University of Naples Federico II, Via D. Montesano, 49, 80131 Naples, Italy*

[2] *Department of Molecular Medicine and Medical Biotechnology, University of Naples Federico II, Via S. Pansini 5, 80131 Naples, Italy*

[3] *Department of Pharmaceutical Sciences, University of Milan, Via Mangiagalli, 25, 20133 Milan, Italy*

[4] *Department of Movement Sciences and Wellness, University of Naples "Parthenope", 80133 Naples, Italy*

[5] *Institute for the Animal Production Systems in the Mediterranean Environment, Via Argine 1085, 80147 Naples, Italy*

ABSTRACT

CDC25 phosphatases play a critical role in the regulation of the cell cycle and thus represent attractive cancer therapeutic targets. We previously discovered the 4-(2-carboxybenzoyl)phthalic acid (NSC28620) as a new CDC25 inhibitor endowed with promising anticancer activity in breast, prostate and leukemia cells. Herein, we report a structure-based optimization of NSC28620, leading to the identification of a series of novel naphthylphenylketone (NPK) and naphthylphenylamine (NPA) derivatives as CDC25B inhibitors. Compounds **7j**, **7i**, **6e**, **7f** and **3** showed higher inhibitory activity than the initial lead, with K_i values in the low micromolar range. Kinetic analysis, intrinsic fluorescence studies and induced fit docking simulations provided a mechanistic understanding of the activity of these derivatives. All compounds were tested in the highly aggressive human melanoma cell lines A2058 and A375. Compound **4a** potently inhibited cell proliferation and colony formation, causing an increase of the G2/M phase and a reduction of G0/G1 phase of the cell cycle in both cell lines.

INTRODUCTION

The cell division cycle 25 phosphatases (CDC25s) are members of the family of dual-specificity phosphatases (DSPs) and regulate cyclin-dependent kinase (Cdk) complexes, which are key participants in the cell cycle.[1, 2] CDC25s are also critical components of the cell cycle checkpoints for handling DNA damage and are inactivated or degraded to induce cell cycle arrest. Misregulation of these processes can cause genomic instability[3, 4] and ultimately lead to cancer. In mammalian cells three variants of CDC25 were identified: CDC25A, -B and -C.[5] CDC25A dephosphorylates Cdk4-Cyclin D[6] and Cdk6-Cyclin D complexes,[7] as well as Cdk1-CyclinB, Cdk2-Cyclin A and Cdk2-Cyclin E complexes,[8, 9] controlling both G1/S and G2/M progression. CDC25B regulates the G2/M transition by activating Cdk1-Cyclin B complex at the centrosome which is subsequently completely activated by CDC25C in the nucleus at the onset of mitosis.[10] Furthermore, CDC25B was reported to dephosphorylate and activate also Cdk2-Cyclin A and Cdk2-Cyclin E complexes.[11, 12] CDC25C regulates the G2/M transition by targeting Cdk1-Cyclin B complex.[13, 14] However, it is believed that all three variants of CDC25 are involved in the regulation of both G1/S and G2/M transitions.[15] CDC25A and CDC25B overexpression is frequently observed in various human cancers, and often associated with more aggressive tumors and poor clinical outcome.[10, 16] Concerning CDC25C, only a few studies showed an overexpression of this form in cancers.[17, 18] However, growing evidence suggests that the overexpression of CDC25C could be underrated because of the non-consideration of its alternative splicing.[19, 20] The overexpression of CDC25s in many human cancers supports their clinical significance and has encouraged the pursuit of specific small molecule inhibitors.

The crystal structures of the catalytic domain of CDC25A (PDB: 1C25)[21] and CDC25B (PDB:1QB0)[22] have been solved at 2.3 Å and 1.9 Å resolution, respectively. Despite the close

structural similarity between the two proteins with regard to the catalytic domain, CDC25A fails to bind oxyanions in its catalytic site, whereas CDC25B readily binds tungstate and sulfate. Moreover, the C-terminal region is well ordered in the crystal structure of CDC25B (residues 531−547), and folded into a well-defined α-helix, while in the CDC25A crystal structure this region is undefined. The active-site region of CDC25A appears in a flat conformation and exposed to bulk solvent, whereas the structure of the catalytic domain of CDC25B reveals a shallow active site cleft, positioned near a large cavity formed by highly hydrophilic moieties in the C-terminal residues of CDC25B, which was referred to as the "swimming pool" due to the abundant presence of many well organized water molecules.[23] Therefore, the structure-based design of inhibitors and the derivation of significant structure-activity relationships (SAR) are really challenging. Nevertheless, several CDC25s inhibitors with different structural features were discovered over the past years, the most potent of which are quinonoid-based derivatives.[24-27] These latter mainly act via irreversible inhibition of CDC25s by electrophilic modification[28, 29] or oxidation of the critical cysteine residue in the catalytic domain by reactive oxygen species (ROS).[30, 31] Furthermore, quinone-containing agents could potentially trigger a range of unrelated events in cells because ROS may oxidize other phosphatases, as well as unrelated cysteine-based enzymes,[26] raising questions about their potential toxicity and limiting their therapeutic applications.[32]

Among the CDC25 inhibitors reported to date, very few display reversible inhibition kinetics. The indolylhydroxyquinone **8L**,[33] the naphthofurandione 5169131,[34] the pyrazolone derivative EK-6136,[35] the thiazolepyrimidine **44**[36] and the aminoisoquinolinone **13**[37] in Figure 1 are some representatives. However, most of the reversible inhibitors have potency within the micromolar range with no currently defined clinical utility. Thus, the identification of non-quinoid reversible inhibitors that do not oxidize cysteine residues or generate ROS

would have great potential for the development of pharmaceutical agents and useful biological tools.

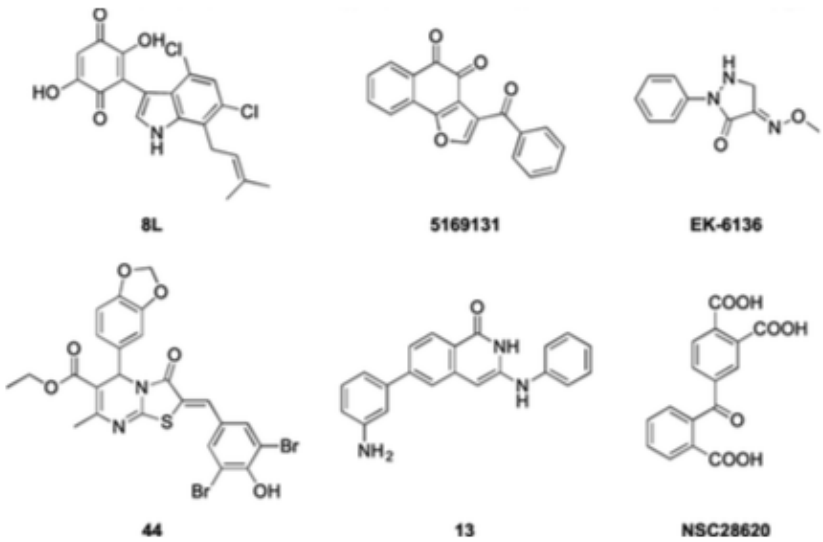

Figure 1. Known reversible CDC25 inhibitors.

We have previously reported the discovery of a new CDC25 inhibitor with cytotoxic activity, the 4-(2-carboxybenzoyl)phthalic acid (NSC28620) by means of a structure-based high-throughput virtual screening.[38] This compound displayed reversible, competitive inhibition kinetics with K_i values of 2.3 and 5.3 μM for CDC25A and -B, respectively, arrested cells at the G0/G1 and G2/M phases of the cell cycle, increased Cdk1 hyperphosphorylation in K562 leukemia cells and significantly inhibited the growth of human MCF-7 breast, PC-3 prostate and K562 leukemia cancer cell lines.

Metastatic melanoma is one of the most aggressive and therapy-resistant human cancers. So, much effort is being directed at discovering new, effective agents for the treatment of this cancer, by targeting various signaling pathways and attacking elements that underlie the tumor's propensity for growth and chemoresistance.[39] Previous studies have reported that Cdk2, Cdk4, Cdk6, cyclins D1, E, and D3 and CDC25A were significantly overexpressed in metastatic melanomas as compared to nevus tissue.[40-42] Moreover, other literature data have indicated that phosphorylation and inhibition of CDC25B cause delayed progression from G2 into mitosis in melanoma cells.[43] Finally, we have recently demonstrated that a small

molecule CDC25 inhibitor was able to arrest melanoma cells in G2/M phase through an intrinsic apoptotic pathway.[27] Taken together, these evidences emphasize that CDC25 could be considered as a possible target in treating melanoma.

Herein we present the results of our lead optimization program, pursued on the CDC25 inhibitor lead NSC28620. Guided by preliminary docking studies, we rationally explored different substitution patterns with the purpose of improving the inhibitory profile of the starting lead and optimizing its potential as antitumor drug. A total of 31 naphthylphenylketone (NPK) and naphthylphenylamine (NPA) derivatives were synthesized (Table 1) and tested according to a SAR investigation by a step-by-step modification strategy. Among them, twelve compounds (**3**, **3b**, **6b**,**d**,**e**, **7d**,**f**,**i**,**j**, **8**, **9** and **12**) displayed an inhibition potency similar or even higher compared to that exerted by the lead compound NSC28620 (Table 1), **7j** being 7-fold more active than NSC28620; the remaining nineteen derivatives conserved a lower but measurable inhibition. The biological effect of these compounds was evaluated in a cellular context, using the highly aggressive human melanoma cell lines A2058 and A375. The data showed that, when tested at a very low concentration, only compound **4a** was by far the most effective one in the inhibition of cell proliferation and colony formation, as emerging from the cytotoxicity tests. Furthermore, compound **4a** affected the cell cycle progression of either A2058 and A375 cells with a significant increase of the G2/M phase and a reduction of G0/G1 phase.

RESULTS AND DISCUSSION

Structure-Guided Optimization of Lead NSC28620 to Target the CDC25B Phosphatase. We used the binding mode of the lead compound NSC28620 into the CDC25B catalytic domain as predicted by docking experiments[38] (Figure 2A) for the rational design of new analogues to study the SAR and to achieve further increases in potency. Four regions in

NSC28620 were explored for modifications (Figure 2B) to design new compounds based upon structural data. First, we explored additional optimization of the phthalic moiety that binds to the swimming pool pocket of CDC25B, a protein region near to the catalytic site and composed by both hydrophobic (F543, L445, M483, W550, P444 and L545) and polar residues (Y428, R479, R482, E446, R544, T547 and S549).

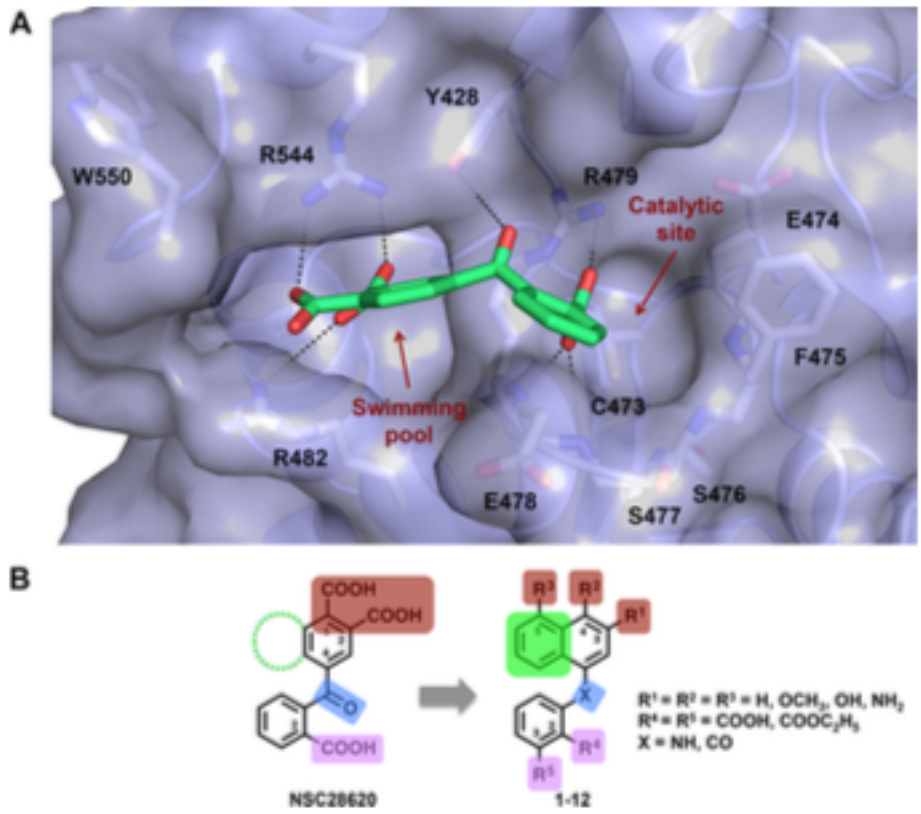

Figure 2. Structure-based optimization of lead NSC28620. (A) Predicted binding mode of NSC28620 (green) in the CDC25B binding cavity. For clarity, only interacting residues are displayed and labeled. Ligand and interacting key residues (white) are represented as stick models, while the protein is a transparent Connolly surface model. H-bonds and salt bridges are shown as dashed black lines. (B) Schematic overview of the rationally designed NSC28620 derivatives.

As depicted in Figure 2A, the two carboxylate groups of the phthalic moiety (positions 1 and 2) of NSC28620 protrude into the swimming pool region and form salt-bridges with both R482 and R544 side chains. In order to explore new potential interactions (hydrophobic and/or hydrophilic) within the swimming pool aimed at improving the inhibition power, we

thoroughly replaced the phthalic system of NSC28620 with a bulkier naphthalene ring system; this moiety was undecorated (compounds **1**-**7**) or decorated with hydroxy, methoxy or amino groups linked to one out of the positions 3, 4 and 5, corresponding to substituents R^1, R^2 and R^3, respectively (compounds **1a-c**, **3a**,**b**, **4a**,**b**, **6a**,**b**,**d**,**e**,**f**, **7a**,**b**,**d**,**e**,**f**,**i**,**j**, **8**, **9**, **10**, **11**, **12**) (Table 1). In the next step, we performed the optimization of the benzoyl substituent interacting with the catalytic site of CDC25B. In the complex of CDC25B with NSC28620, the carboxylate group of the benzoyl moiety binds deep in the catalytic site, making a salt-bridge with the R479 guanidinium group and a H-bond with the catalytic backbone NHs of R479 and E478. This moiety occupies the same location as the sulfate ion bound to the catalytic site of the CDC25B crystal structure.[22] Therefore, we sought to explore the role of the carboxylic acid function at position 2 or 3 of the benzoyl moiety (substituents R^4 and R^5, respectively) in order to establish more favorable interactions within the catalytic domain (compounds **1**, **1a-c**, **6**, **6a**,**b**,**d**,**e**,**f**, **7**, **7a**,**b**,**d**,**e**,**f**,**i**,**j** and **12**). Moreover, according to the well-known Caco-2 uptake studies[44], demonstrating the enhanced permeability of esters compared to their corresponding acids, the carboxylic acidic moiety was modified via esterification with the aim of increasing the lipophilicity and enhancing the cellular uptake (compounds **2**, **3**, **3a**,**b**, **4**, **4a**,**b**, **8**, **9**, **10**, **11**). Finally, the NSC28620•CDC25B complex revealed that the carbonyl group of the inhibitor accepts a H-bond from the Y428 OH group (Figure 2A). On the basis of the structural model, we replaced the carbonyl group (position X) with an amino group with the overall goal to explore the H-bond acceptor or donor capability at this position (compounds **3**, **3a**,**b**, **4**, **4a**,**b**, **5**, **6**, **6a**,**b**,**d**,**e**,**f**, **7**, **7a**,**b**,**d**,**e**,**f**,**i**,**j**, **8**, **9**, **10**, **11**, and **12**).

Synthesis of Rationally Designed NPK and NPA Derivatives. The general synthetic strategy followed for the preparation of NPK derivatives is outlined in Scheme 1 and Scheme 2. Grignard's reagent was prepared *in situ* starting from the commercially available 1-

bromonaphthalene in presence of magnesium turnings. The organomagnesium halide was added to a solution of phthalic anhydride in dry tetrahydrofuran to afford compound **1**.[45] The subsequent Fischer esterification of the carboxylic group in ethanol with sulfuric acid as catalyst provided the final ester **2** (Scheme 1).[46]

Scheme 1. Synthesis of 2-(1-Naphthoyl)benzoic Acid 1 and Its Ethyl Ester 2[a]

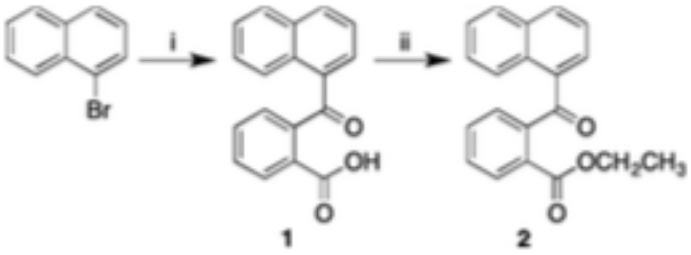

[a]Reagents and conditions: (i) (a) Mg, dry THF, N_2, reflux, 1 h; (b) phthalic anhydride, dry THF, N_2, reflux, 48 h; (ii) EtOH, H_2SO_4, reflux, 24 h.

Otherwise, in order to obtain the same class of compounds previously described but bearing a hydroxyl group on the naphthalene ring, a second synthetic approach was developed (Scheme 2).

The 1-aminonaphthalene (**24**), by halogenation with bromine in acetic acid, provided the intermediate **13** whose treatment with sodium nitrite led to the formation of the diazonium salt **14**,[47] which was isolated and characterized. The conversion of **14** into the 4-bromo-2-hydroxynaphthalene **15a** was performed with sodium borohydride. This latter or the commercially available 4-bromo-1-hydroxynaphthalene (**15b**) were subsequently protected as methyl ether in the presence of iodomethane to provide the intermediates **16a,b**. Finally, the exchange of the halogen atom with lithium by treatment with a solution of *n*-butyllithium (*n*-BuLi) dry THF at -78°C, followed by the formylation with *N,N*-dimethylformamide, led to the naphthaldehydes **17a,b** (Scheme 2).

On the other hand, the key intermediate **20**[48] was obtained by condensation of the commercially available 2-bromobenzoic acid with 2-amino-2-methyl-1-propanol to afford the

intermediate **18**. This latter was reacted with thionyl chloride in diethyl ether to give the oxazoline **19**, which underwent a metal-halogen exchange in the presence of the organolithium species *n*-BuLi to afford **20**.

Compound **20** reacted with the appropriate substituted naphthaldehydes **17a,b** and the acid-catalyzed deprotection of the carboxylic moiety led to the desired lactones **21a,b** in alkaline condition. The oxidation of these latter with potassium permanganate and 25% aqueous solution of KOH in pyridine afforded the 2-(methoxy-1-naphthyl)benzoic acids **1a** and **1b**. Finally, the cleavage of the methyl ether of **1a** with a 1M solution of boron tribromide in dichloromethane provided the final product **1c** (Scheme 2).

Scheme 2. Synthesis of 2-(3(4)-Methoxy-1-naphthyl)benzoic Acids 1a, b, and 2-(3-Hydroxy-1-naphthoyl)benzoic Acid 1c[a]

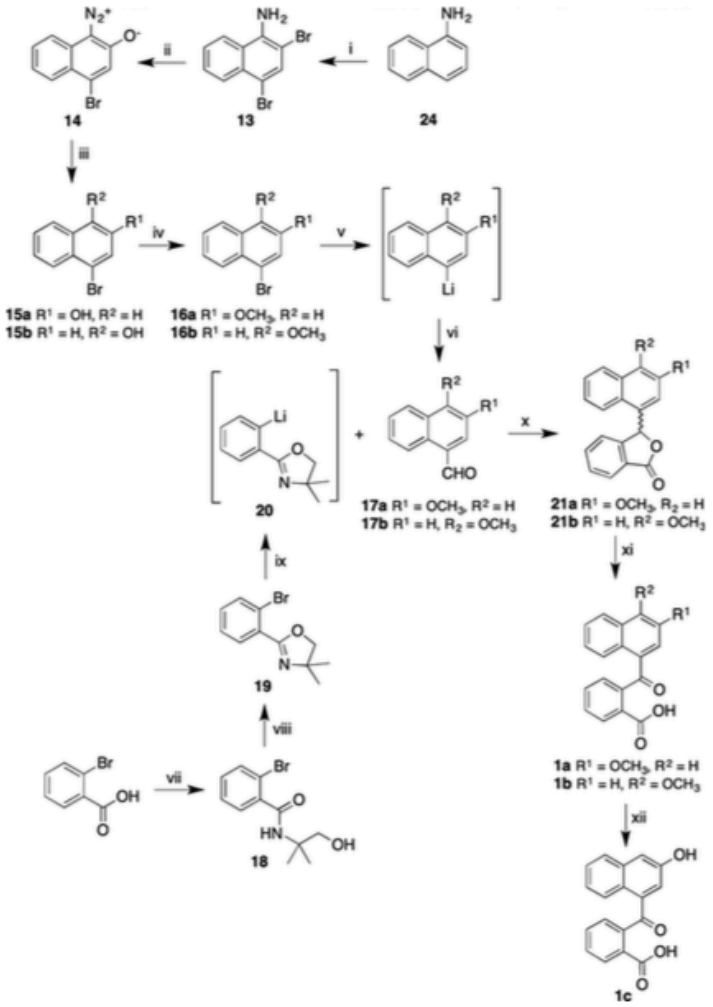

[a]Reagents and conditions: (i) Br_2, AcOH, 60 °C, 15 min; (ii) $NaNO_2$, AcOH, 8−10 °C, 10 min; (iii) $NaBH_4$, EtOH, 0−10 °C, 2−3 h; (iv) (a) NaH, dry DMF, N_2, rt, 15 min; (b) CH_3I, dry DMF, N_2, rt, 3 h; (v) *n*-BuLi, dry THF, N_2, −78 °C, 1 h; (vi) dry DMF, dry THF, N_2, −78 °C, 1 h; (vii) (a) $SOCl_2$, N_2, reflux, 6 h; (b) 2-amino-2-methyl-1-propanol, dry dichloromethane (DCM), N_2, rt, 2 h; (viii) (a) $SOCl_2$, N_2, rt, 30 min; (b) dry Et_2O, 30 min; (c) 20% NaOH; (ix) *n*-BuLi, dry Et_2O, N_2, −78 °C, 1 h; (x) (a) dry Et_2O, N_2, rt, overnight; (b) 3 M HCl, reflux, 4.5 h; (c) 10% NaOH, reflux, 1 h; (xi) 25% KOH, $KMnO_4$, Py, reflux, 5 h; (xii) BBr_3 (1 M in DCM), dry DCM, N_2, rt, 30−210 min.

In parallel, the synthesis of NPA derivatives was carried out (Schemes 3 and 4). The appropriate substituted aryl halide and aryl amine underwent a palladium-catalyzed Buchwald amination reaction[49] (compounds **3, 3a-c, 3h, 4, 4a-c, 4g,h** and **5**) using a mixture of palladium acetate ($Pd(OAc)_2$) and racemic 2,2'-bis(diphenylphosphino)-1,1'-binaphthalene (BINAP) as catalysts, in the presence of Cs_2CO_3. Since the yield of the aryl amination reaction was critically hindered by the electron deficiency of the amine, the combination of the more nucleophilic amine and more electrophilic aryl bromo derivatives was used (procedures C1 and C2, Scheme 3).

The appropriate bromo naphthylamines for the synthesis of **4g,h** were *N*-protected with di-*tert*-butyl dicarbonate.[50] The protection of the substituted benzoic acids to obtain ethyl-2(3)-bromobenzoate (**22**, **23**) was performed by Fischer esterification.[51]

Scheme 3. Synthesis of Ethyl-(naphthylamino)benzoates 3, 3a–c, 3h, 4, 4a–c, 4g, h, and 5[a]

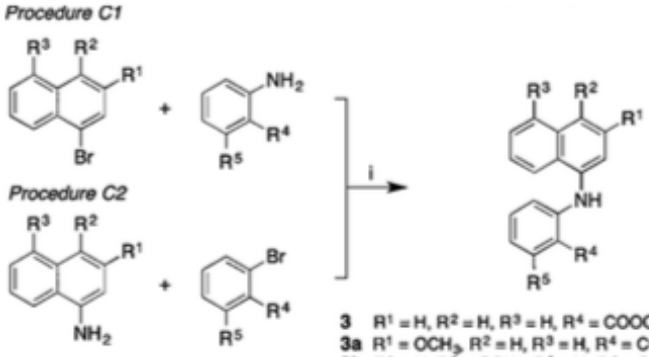

		Procedure
3	$R^1 = H, R^2 = H, R^3 = H, R^4 = COOC_2H_5, R^5 = H$	C1
3a	$R^1 = OCH_3, R^2 = H, R^3 = H, R^4 = COOC_2H_5, R^5 = H$	C1
3b	$R^1 = H, R^2 = OCH_3, R^3 = H, R^4 = COOC_2H_5, R^5 = H$	C2
3c	$R^1 = H, R^2 = H, R^3 = OCH_3, R^4 = COOC_2H_5, R^5 = H$	C2
3h	$R^1 = H, R^2 = H, R^3 = NHBoc, R^4 = COOC_2H_5, R^5 = H$	C1
4	$R^1 = H, R^2 = H, R^3 = H, R^4 = H, R^5 = COOC_2H_5$	C1
4a	$R^1 = OCH_3, R^2 = H, R^3 = H, R^4 = H, R^5 = COOC_2H_5$	C1
4b	$R^1 = H, R^2 = OCH_3, R^3 = H, R^4 = H, R^5 = COOC_2H_5$	C1/C2
4c	$R^1 = H, R^2 = H, R^3 = OCH_3, R^4 = H, R^5 = COOC_2H_5$	C2
4g	$R^1 = H, R^2 = NHBoc, R^3 = H, R^4 = H, R^5 = COOC_2H_5$	C1
4h	$R^1 = H, R^2 = H, R^3 = NHBoc, R^4 = H, R^5 = COOC_2H_5$	C1
5	$R^1 = H, R^2 = H, R^3 = H, R^4 = H, R^5 = H$	C1

[a]Reagents and conditions: (i) $Pd(OAc)_2$, (±)-BINAP, Cs_2CO_3, dry toluene, Ar, 80 °C, 17–40 h.

A basic hydrolysis of the ester group was then performed, leading to the formation of the corresponding acids **6, 6a-c, 7, 7a-c, 7g,h** and **12** (Scheme 4)[52]. The cleavage of methoxy protection was performed with a 1M solution of boron tribromide in dichloromethane to afford compounds **6d-f** and **7d-f** (Scheme 4). The *N*-Boc protecting group of compounds **7g** and **7h**, was hydrolyzed with HCl (4M in 1,4-dioxane) to give compounds **7i**,**j** while by using

trifluoroacetic acid products **10** and **11** were obtained (Scheme 4). From the deprotected intermediate **10**, using the same conditions, product **12** was obtained (Scheme 4). The esters **8** and **9** were achieved by esterification of compounds **6f** and **7f** respectively, in acid conditions by microwave irradiation (Scheme 4).

Scheme 4. Synthesis of (Naphthylamino)benzoic Acid Derivatives 6, 6a–f, 7, 7a–j, and 8–12[a]

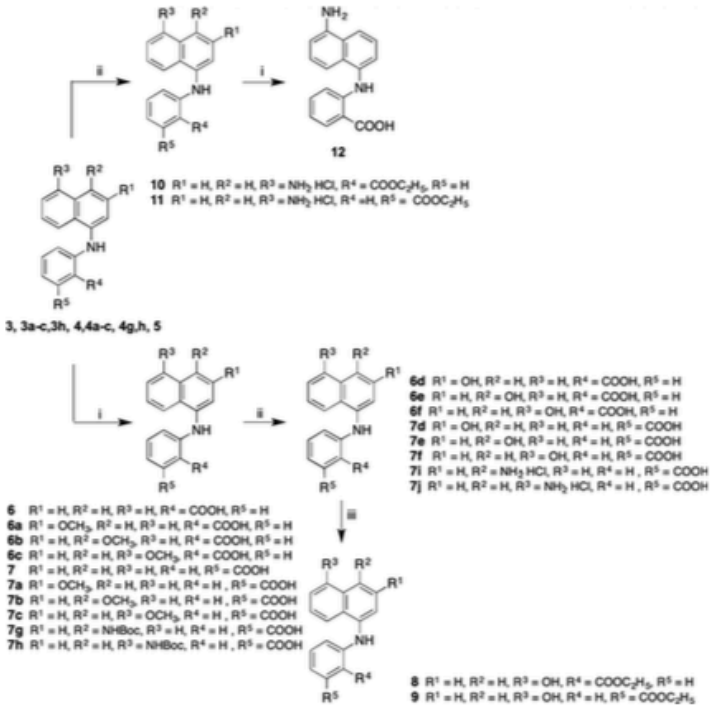

[a]Reagents and conditions: (i) 1 M NaOH, THF/EtOH (1:1), reflux, 30–90 min; (ii) (a) HCl (4 M in 1,4-dioxane), dry 1,4-dioxane, r.t., 24 h, or trifluoroacetic acid, dichloromethane, r.t., 60 min (for **10** and **11**); (b) BBr_3 (1 M in dichloromethane), dry dichloromethane, N_2, r.t., 30–210 min; (iii) H_2SO_4, EtOH, MW 80 °C, 90 min (for **8** and **9**).

Effect of NPK and NPA Derivatives on the Phosphatase Activity of Purified Recombinant Form of CDC25B. The evaluation of the inhibition properties exhibited by the NPK and NPA derivatives was carried out through kinetic measurements of the phosphatase activity sustained by the recombinant form of CDC25B. In particular, the hydrolysis rate of the synthetic substrate 3-O-methylfluorescein phosphate (OMFP) triggered by CDC25B was measured at different substrate concentrations, in the absence or in the presence of various inhibitor concentrations. The resulting data of initial velocity (v_i) were analyzed in Lineweaver-Burk plots, thus allowing an inspection on the inhibition mechanism possessed by the novel compounds. As reported in Table S1 (Supporting information), the

affinity for the substrate OMFP measured in the absence of inhibitor (K_M = 2.7 ± 0.2 μM), remained essentially unvaried in the presence of some inhibitors, decreased with other inhibitors or slightly increased with the remaining ones. On the other hand, the maximum velocity of OMFP hydrolysis measured in the absence of inhibitor (V_{max} = 323 ± 10 AU/min) significantly decreased in the presence of the indicated concentrations of all synthesized compounds. These findings differ from the data already reported for NSC28620, because this compound caused an increase of the K_M without any variation of the V_{max}, a typical behavior for a competitive inhibition of CDC25B.[38] Therefore, none of the analyzed compounds may be ranked as a competitive inhibitor of CDC25B; probably, the addition of a bulky benzene ring in all derivatives causes a variation in the binding mode of the inhibitors to CDC25B. However, this different interaction drives in some cases to a stronger inhibition of CDC25B (Table 1). An inspection of the kinetic data allowed a putative assignment of the compounds to different categories of inhibition mechanism. Hence, inhibitors were classified as non-competitive (Figure S1 of Supporting Information), un-competitive (Figure S2 of Supporting Information) or mixed (Figure S3 of Supporting Information) on the basis of the comparison of the Lineweaver-Burk plots obtained in the presence of different inhibitor concentrations with that obtained in the absence of inhibitor. For instance, as depicted in Figure 3A, **7j** appears as a typical non-competitive inhibitor, because the progressive decrease of the V_{max} at increasing inhibitor concentration occurs without a significant change of the K_M for OMFP (see also Table S1). On the other hand, **3** exhibits a kinetic behaviour approaching that of an un-competitive inhibitor, because the progressive decrease of V_{max} appears to be concomitant to a roughly similar decrease of the K_M (Figure 3B and Table S1).

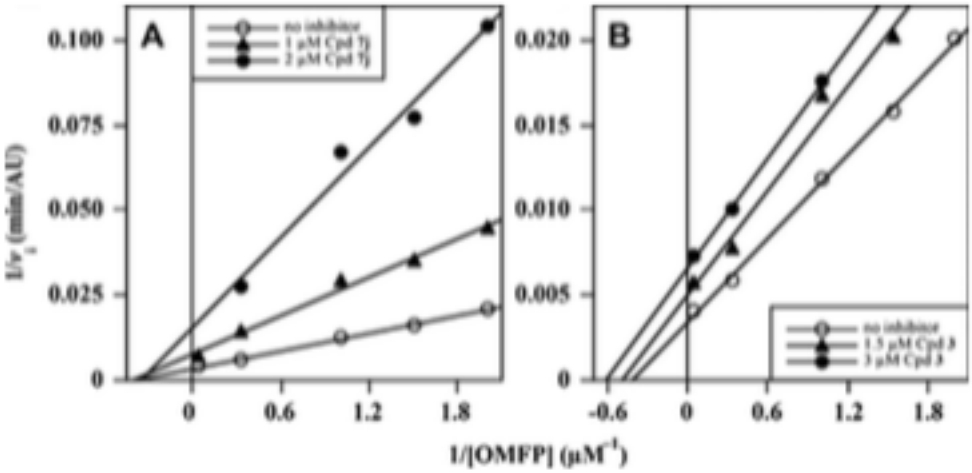

Figure 3. Effect of compound 7j or 3 on the Lineweaver–Burk plots of the CDC25B phosphatase activity. The activity, measured through the OMFP hydrolysis rate as described in the Experimental Section, was determined in the absence (open circles in both panels) or in the presence of 1.0 μM or 2.0 μM compound 7j (filled triangles or filled circles, respectively; panel A) or 1.5 or 3.0 μM compound 3 (filled triangles or filled circles, respectively; panel B).

This kinetic approach allowed the calculation of the inhibition constant (K_i) for each derivative on the basis of the varied kinetic parameters resulting from the inhibition. The K_i values (Table 1) are comprised in a large interval ranging from 0.8 μM to 69 μM, thus indicating that the inhibition properties of this series of compounds are dependent on the modifications realized through the optimization program. In particular, some derivatives (such as **7j**, **7i**, **6e**, **7f** or **3**) are endowed with a significantly stronger inhibition potency compared to that of the initial lead NSC28620 (K_i = 5.3 μM), whereas the remaining compounds display a comparable or lower inhibition.

Table 1. Rationally Designed Compounds 1−12 and Their Inhibition Kinetic Parameters against CDC25B

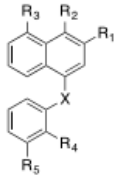

1-12

Cpd	R^1	R^2	R^3	R^4	R^5	X	K_i[a] (μM)	putative inhibition mechanism
1	H	H	H	COOH	H	CO	69	mixed
1a	OCH_3	H	H	COOH	H	CO	36	mixed
1b	H	OCH_3	H	COOH	H	CO	7.1 ± 0.9	non-competitive
1c	OH	H	H	COOH	H	CO	34 ± 3	non-competitive
2	H	H	H	$COOC_2H_5$	H	CO	54	mixed
3	H	H	H	$COOC_2H_5$	H	NH	2.8 ± 0.7	un-competitive
3a	OCH_3	H	H	$COOC_2H_5$	H	NH	12.5 ± 2.6	un-competitive
3b	H	OCH_3	H	$COOC_2H_5$	H	NH	6.9 ± 2.0	non-competitive
4	H	H	H	H	$COOC_2H_5$	NH	7.3 ± 0.6	un-competitive
4a	OCH_3	H	H	H	$COOC_2H_5$	NH	8.5 ± 1.2	un-competitive
4b	H	OCH_3	H	H	$COOC_2H_5$	NH	11.9 ± 4.2	non-competitive
5	H	H	H	H	H	NH	32	mixed
6	H	H	H	COOH	H	NH	22 ± 3	un-competitive
6a	OCH_3	H	H	COOH	H	NH	16.9 ± 0.3	non-competitive
6b	H	OCH_3	H	COOH	H	NH	6.1 ± 0.7	un-competitive
6d	OH	H	H	COOH	H	NH	5.1 ± 0.7	non-competitive
6e	H	OH	H	COOH	H	NH	2.7 ± 1.1	non-competitive
6f	H	H	OH	COOH	H	NH	13.4 ± 1.1	non-competitive
7	H	H	H	H	COOH	NH	30	mixed
7a	OCH_3	H	H	H	COOH	NH	55 ± 7	un-competitive
7b	H	OCH_3	H	H	COOH	NH	45 ± 3	un-competitive
7d	OH	H	H	H	COOH	NH	5.8 ± 0.8	non-competitive
7e	H	OH	H	H	COOH	NH	6.4 ± 0.8	un-competitive
7f	H	H	OH	H	COOH	NH	2.9 ± 0.3	non-competitive
7i[b]	H	NH_2	H	H	COOH	NH	1.4 ± 0.3	non-competitive
7j[b]	H	H	NH_2	H	COOH	NH	0.8 ± 0.2	non-competitive
8	H	H	OH	$COOC_2H_5$	H	NH	7.4 ± 2.2	non-competitive
9	H	H	OH	H	$COOC_2H_5$	NH	4.9 ± 1.3	non-competitive
10[b]	H	H	NH_2	$COOC_2H_5$	H	NH	9.9 ± 3.2	non-competitive
11[b]	H	H	NH_2	H	$COOC_2H_5$	NH	36 ± 3	non-competitive
12	H	H	NH_2	COOH	H	NH	6.5 ± 1.4	non-competitive
NSC28620[38]							5.3 ± 2.4	competitive

[a]The values of K_i, calculated as indicated in the Experimental Section, are an average from at least three independent experiments. The missing standard deviation for mixed inhibitors is due to the fact that the K_i value indicated is just a rough evaluation of the inhibition power. [b]Compounds were tested as hydrochloride salts.

Most of the CDC25B inhibitors, including the lead compound NSC28620, are also active against CDC25A and CDC25C (refs 27, 38). Hence, an evaluation of the inhibition properties of some NPA derivatives towards the recombinant forms of both CDC25A and -C was considered. In particular, we have checked the inhibition potency of the most potent non-competitive and un-competitive inhibitor, i.e. **7j** and **3**, respectively. Using the same approach and experimental conditions adopted for CDC25B, the kinetic parameters K_M and V_{max} measured for CDC25A in the absence of inhibitors were 2.0 µM and 217 AU/min, respectively; these values were quite similar to those obtained for CDC25B. On the other hand, the corresponding K_M and V_{max} measured for CDC25C were 16 µM and 182 AU/min,

thus indicating that this CDC25 form exhibits a lower catalytic efficiency, essentially due to a lower affinity for the synthetic substrate OMFP. The kinetic measurements obtained in the presence of the inhibitors **7j** and **3** indicated that both compounds were active also on CDC25A and -C. In particular, the K_i of **7j** towards CDC25A and -C was 0.6 μM and 4.0 μM, respectively, whereas the corresponding K_i of **3** was 0.6 μM and 0.4 μM, respectively. In the complex, the analysis of the inhibition parameters related to the three CDC25 forms could reflect slight differences in the binding mode of substrate and/or inhibitor, as already reported for other CDC25 inhibitors (refs 27, 38).

SAR Investigation. The biochemical evaluation of the inhibitory effects of the thirty-one compounds against CDC25B allowed a comprehensive description of the SAR for both NPK and NPA scaffolds. Derivatives bearing a carbonyl group as linker were all less active than the lead compound NSC28620 (**1**, **1a**, **1c** and **2**), with only compound **1b** showing a nearly comparable activity. Indeed, the replacement of the carbonyl group with a secondary amino group in the X position caused an overall improvement of the inhibition power of this series of derivatives, as emerging from the comparison of the K_i values of **1** vs **6** (69 vs 22 μM), **1a** vs **6a** (36 vs 16.9 μM), **1c** vs **6d** (34 vs 5.1 μM), or **2** vs **3** (54 vs 3.7 μM).

Then, we analyzed the effects observed for the compounds bearing the carboxylic acid moiety at R^5 (derivatives **7** and **7a**,**b**,**d-f**,**i**,**j**). The unsubstituted derivative **7**, as well as compounds bearing the methoxy group at R^1 (**7a**) or R^2 (**7b**) showed poor inhibitory activity (K_i 30, 55 or 45 μM in **7**, **7a** or **7b**, respectively). Instead, the introduction of polar substituents caused an interesting increase in inhibition potency. Indeed, the presence of the hydroxyl group at R^1 (**7d**), R^2 (**7e**), and even more at R^3 position (**7f**) significantly enhanced the inhibition power, as reflected by the decrease of the K_i value in the order: 30 μM in **7** >> 5.8 μM in **7d** ~ 6.4 μM in **7e** > 2.9 μM in **7f**. Furthermore, the introduction of the amino

group at R^2 in **7i** and even more at R^3 in **7j** provoked a further increase of the inhibition power (1.4 μM in **7i** and 0.8 μM in **7j**), leading to the most potent compound of the whole series of inhibitors. Moreover, **7j** was 7-fold more active than the initial lead NSC28620. Therefore, the presence of one polar group (hydroxyl or amino) on the naphthalene system of inhibitors carrying a carboxylic group at R^5 significantly increased their capability of inhibiting the CDC25B phosphatase activity.

A somehow similar trend was observed when the free carboxylic moiety was moved at position R^4 (derivatives **6**, **6a**,**b**,**d-f**, **12**). The unsubstituted derivative **6** had a low inhibition activity (K_i 22 μM), similar to that obtained after the introduction of the methoxy group at position R^1 in **6a** (K_i 16.9 μM); however, when this group was moved at R^2 in **6b**, a remarkable increase of the inhibition potency was observed (K_i 6.1 μM). Instead, the presence of the hydroxy group at R^2 in **6e** conferred the highest potency in this series (K_i 2.7 μM), but shifting this group at R^1 in **6d** or even more at R^3 in **6f** caused a decrease in potency (K_i 5.1 μM in **6d** and 13.4 μM in **6f**). Instead, derivative **12**, where position R^3 was occupied by an amino group, showed an improved inhibition (K_i 6.5 μM) compared to **6d**.

In some derivatives the esterification of the carboxylic group at R^4 (**3**, **3a-b**, **8**, **10**) or R^5 (**4**, **4a-b**, **9**, **11**) position was performed in order to increase the lipophilicity of the compound. Among the ester series at R^4, the unsubstituted derivative **3** showed the highest potency (K_i 3.7 μM). No improvement of the inhibition power was obtained with the introduction of a methoxy group at position R^1 in **3a** or R^2 in **3b**, or with the presence of a polar substituent, such as hydroxyl or amino group at position R^3 in **8** or **10**, respectively. Instead, the K_i value of the substituted derivatives raised to 12.5 μM in **3a**, or slightly increased to 6.9 μM in **3b**, 7.4 μM in **8** or 9.9 μM in **10**. Therefore, the activity of these compounds is not improved by the presence of different substituents on the naphthalene moiety.

Moving to the ester function at R^5, in four out of five derivatives the inhibition power was essentially similar to that exhibited by the corresponding ester analogues at R^4. In particular, the unsubstituted derivative **4** displayed a slightly lower potency (K_i 7.3 μM) than the analogue **3**. Derivatives bearing the methoxy group at R^1 (**4a**) or R^2 (**4b**) showed potency in the same range (8.5 and 11.9 μM, respectively) of the analogues **3a** and **3b**. A slight improvement of the potency (K_i 4.9 μM) was obtained upon the introduction of the hydroxyl group at R^3 in **9**; in contrast, the presence of the amino group at this position was, surprisingly, detrimental (K_i 36 μM in **11**).

In conclusion, the presence of the NPA scaffold appears to be sufficient to attain the best inhibition, when the carboxylic group at R^4 or R^5 was esterified.

Intrinsic Fluorescence of the CDC25B Catalytic Domain Upon the Addition of Typical NPA Derivatives. The amino acid sequence of the catalytic domain of CDC25B includes one tryptophan (W550) and eleven tyrosine residues (Y382, Y400, Y428, Y430, Y432, Y497, Y501, Y502, Y506, Y512 and Y528).[22] In particular, W550 is located in the protein region known as "swimming pool" for the great number of water molecules found in the crystal structure.[22] These findings prompted an investigation on the intrinsic fluorescence of the purified recombinant CDC25B; Figure 4 shows the emission spectrum obtained at the excitation wavelength of 280 nm (black line). The emission maximum at 357 nm is likely due to the intrinsic fluorescence of W550, whereas the shoulder around 310 nm is probably due to the emission of the eleven tyrosine residues. This hypothesis was confirmed by the emission spectrum recorded at 295-nm excitation wavelength. Under this condition, a drastic reduction of the tyrosine emission was obtained and, as predicted, the shoulder at 310 nm essentially disappeared, whereas the emission maximum at 357 nm was still present, although reduced in quantum yield (not shown). These findings indicate a clear distinction between tryptophan

and tyrosine emission; furthermore, the position of the emission peak at 357 nm is typical of the great exposure of W550 to the water environment, thus suggesting that this residue lays on the edge of the swimming pool.

The effect of the inhibitors on the intrinsic fluorescence of CDC25B was investigated by adding some NPA derivatives causing a measurable inhibition of the CDC25B phosphatase activity. In particular, compounds **7j** and **7i**, typical non-competitive inhibitors, were added at 1.5 μM and 3 μM respectively, whereas the un-competitive inhibitors **3** and **4a** were added at 4 μM and 10 μM, respectively. The chosen concentrations reflected the different inhibition potency of the various inhibitors. As shown in Figure 4, **7j** (purple line) and **7i** (green line) caused an evident quenching of the fluorescence yield, without shifting the emission maximum at 357 nm. On the other hand, the addition of **3** (red line) or **4a** (blue line) was ineffective in altering the CDC25B emission maximum. A possible explanation for the different behavior of the inhibitors is hereafter reported. Indeed, the non-competitive inhibitors **7j** and **7i** could directly bind to CDC25B and this interaction caused a conformational change in the region containing W550. On the other hand, the un-competitive inhibitors **3** and **4a** could be unable to directly bind to the enzyme, because binding of these compounds should require the preformed enzyme•substrate complex. Obviously, the substrate OMFP was omitted in fluorescence experiments, owing to its fast hydrolysis.

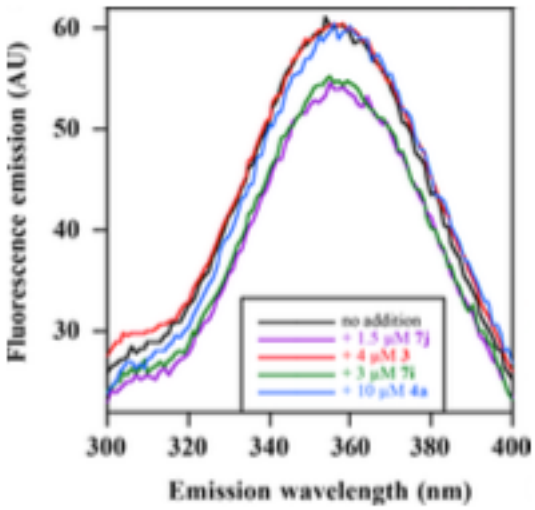

Figure 4. Effect of some NPA derivatives on the intrinsic fluorescence of CDC25B. The emission spectrum of 1 μM recombinant CDC25B in 20 mM Tris·HCl, pH 7.8 buffer containing 0.5 mM TCEP and 0.5% (v/v) DMSO was recorded at 20 °C using the excitation wavelength of 280 nm, either in the absence (black line) or in the presence of 1.5 μM **7j** (purple line), 3 μM **7i** (green line), 4 μM **3** (red line), or 10 μM **4a** (blue line).

Docking Studies. Among the thirty-one synthesized derivatives, compounds **7j** and **3** are representative members of a different binding interaction with CDC25B, as emerging from the kinetic and fluorescence studies. Extensive efforts trying to co-crystallize CDC25B with **7j** and **3** or to soak **7j** and **3** into crystals of CDC25B were unsuccessful. We next carried out docking experiments into the CDC25B crystal structure (PDB ID: 1QB0)[22] in an attempt to determine the binding mode of these two NPA derivatives and to rationalize the observed SAR data. Under this concern, we have the information of the kinetic data, indicating that **7j** and **3** are non-competitive and un-competitive inhibitor, respectively. This means that **7j** and **3** must, by definition, be able to bind in a site distinct from the substrate active site and leave the active site unblocked. However, **7j** should equally react with free enzyme or the enzyme•substrate complex, whereas **3** should react only with the complex. In addition, several CDC25B inhibitors identified by other groups have been proposed to bind into the swimming pool,[23, 34, 53-55] that is a deep and concave pocket between the C-terminal helix A

and the P-loop and does not face the catalytic site directly. Another useful information for docking experiments comes from the fluorescence studies, suggesting that **7j** directly binds to CDC25B in a region affecting the emission of W550, the residue located in the C-terminal helix lining the swimming pool. Vice versa, **3** seems to be unable to directly bind to the free enzyme. Hence, our docking studies were focused on the swimming pool site.

Analysis of the available crystal structures of the native catalytic domain of CDC25B (Figure S4 of Supporting Information) showed that several residues of the swimming pool (W550, R548, R544, F543, L540, N532, Y428, E446, R482), as well as residues that surround the active site cleft exhibit much higher B-factors, which is indicative of their higher flexibility. In particular, R482, which plays an important role in the catalytic activity of the enzyme,[56] showed the highest degree of mobility. Thus, **7j** and **3** were docked to the structure of CDC25B using the Induced Fit Docking (IFD) protocol of the Schrödinger suite,[57, 58] that is intended to circumvent the inflexible binding site and accounts for the side chain (Figure S4 of Supporting information) or backbone movements or both upon ligand binding. Docking results were validated with the metadynamics method described by Clark et al., which allows accurate and reliable predictions of protein•ligand binding poses at a feasible computational cost.[59]

As illustrated in Figure 5A, the top-ranked solution for the most potent non-competitive inhibitor **7j** was deeply inserted into the swimming pool, with the carboxylic acid moiety forming two strong salt-bridges with R482 and R544. This latter formed an additional cation-π interaction with the naphthalene moiety of the ligand. Notably, both arginine residues are involved in the recognition of the Cdk phosphate group and were previously described to be critical for the binding of CDC25 inhibitors by both site-directed mutagenesis[60] and computational studies.[55, 61] In addition, the participation of R482 and R544 in the binding of CDC25B inhibitors was also revealed by the crystal structure of CDC25B in complex with a

modified peptide.[62] The secondary amino group at position X of the NPA derivative engaged a H-bond with the side chain of E446, whereas the amino group at position R^3 formed contacts with C426 (the "back-door cysteine")[22] through a H-bond with the CO backbone. The inhibitor established further hydrophobic interactions with the side chains of M483, Y428 and W550, as also confirmed through the fluorescence studies. In summary, **7j** lies within the swimming pool pocket and does not interfere with the substrate binding in the active site, thus explaining the non-competitive nature of the inhibition, as determined through kinetic analyses. Therefore, the interaction of the carboxylic acid moiety in **7j** and its congeners with R482 and R544 may explain the increased inhibitory potency towards CDC25B. This model also suggests that the differences in potencies observed when the polar amino group was moved to another position on the naphthalene moiety (**7i**), or replaced by the hydroxyl group in various positions (**7d,e,f**), could be due to a less efficient interaction with residue C426.

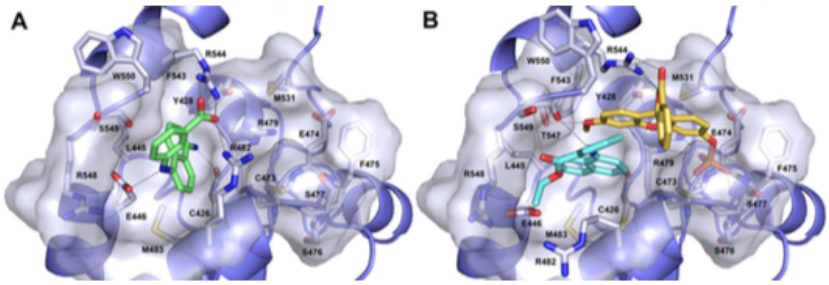

Figure 5. (A) Binding mode of compound 7j (green) into the swimming pool site of CDC25B (PDB ID: 1QB0). (B) Binding mode of compound **3** (cyan) to CDC25B in complex with the artificial OMFP substrate. For clarity, only interacting residues are displayed and labeled. Ligands and interacting key residues (white) are represented as stick models, while the protein is a slate ribbon model. The catalytic site and the adjacent deeper and larger swimming pool site are displayed as a bluewhite Connolly surface. H-bonds and salt bridges are shown as dashed gray lines.

Next, we went on to characterize the binding mode of the most potent un-competitive inhibitor **3**. Taking into account that such inhibition mechanism implies the binding of the inhibitor to the enzyme•substrate complex, a model of the artificial substrate OMFP bound to CDC25B was first generated. Therefore, OMFP was docked to the structure of CDC25B using the IFD protocol and the binding pose metadynamics was employed to select the most stable pose consistent with the catalytic mechanism. As depicted in Figure 5B, the phosphoryl group of the artificial substrate was found to bind within the active site pocket of

CDC25B, where it formed interactions with the residues of the P-loop containing the catalytic cysteine (C473). The orientation of the phosphoryl group mimicked exactly the structure of the bound sulfate, mimicking a bound phosphorylated substrate, in the CDC25B crystal structure.[22] The xanthene moiety of OMFP protruded into the swimming pool and formed H-bonds with Y428 and T547 residues as well as a π-cation interaction with R544, whereas the spirobenzofuranone system was engaged in H-bonds with the side chain of R544. The interaction between aromatic rings of OMFP and the M531, Y428, F543 and W550 side chains further contributed to the binding through hydrophobic stabilization.

The newly generated CDC25B•OMFP complex was employed for further docking of **3**. The resulting top-ranked binding mode, which places **3** directly in the swimming pool near the bound substrate OMFP, is consistent with its un-competitive mode of inhibition. In particular, the naphthalene ring of **3** was sandwiched between R482 and the xanthene moiety of OMFP, with this latter forming a π-stacking interaction. In addition, **3** engaged further hydrophobic interactions with M483 and L445, whereas the phenyl ring holding the ester function at position 2 also stacked against the spirobenzofuranone ring of OMFP. The linker amino group and the carbonyl ester of the inhibitor was engaged in H-bonds with the CO backbone and the side chain of S549, respectively, while the ethyl-ester group interacted with the non-polar side chain carbons of R548.

Therefore, the upper wall of the swimming pool together with the substrate OMFP provide a hydrophobic environment critical for binding of the bulky NPA scaffold of **3**. Indeed, the inhibition of CDC25B by **3** seems to occur when the binary enzyme•OMFP complex is formed. Moreover, as evidenced by SAR data, the binding affinity of this series of compounds is less influenced by the nature and position of substituents on the naphthalene ring. Indeed, the unsubstituted **3** tightly fits in the hydrophobic cleft lined by the swimming

pool and OMFP, whereas the introduction of a methoxy group at R^1 (**3a**) is disfavored due to steric clashes with E478 and R479.

The lower affinity of **3** and its congeners compared to **7j** seems to be due to the presence of the ester function in place of the acidic one: in the first case the ester function forms only weak hydrophobic interactions with the enzyme, while in the second case the free acidic group is involved in strong salt-bridges with the key arginine residues within the swimming pool. For these reasons, **3** adopts a different binding mode that generates a side-chain reorientation into the swimming pool pocket, likely disrupting the network of interactions critical for the catalytic activity of the enzyme.

Effects of the NPK and NPA Derivatives on Cell Growth Rate of Melanoma Cells. We previously documented that the lead NSC28620 affected the cell cycle, increased the levels of the inactive p-Cdk1, as well as reduced the cell viability of some cancer cell lines.[38] We next evaluated the effects of the novel NPK and NPA derivatives in the metastatic human melanoma cell line A2058, a highly resistant and aggressive cancer type. In a preliminary screening, the effect of these compounds, added at 50 μM, was assessed after different times of treatment, using the MTT assay. After 24 h, only **4a** caused an evident cytotoxic activity, but when the analysis was prolonged, also another compound, *i.e.* **4**, resulted cytotoxic after 48-h treatment (not shown).

To check the minimum concentration of **4** and **4a** leading to a reduction of the cell growth rate, the time-dependent effect of these compounds on A2058 melanoma cells was tested at lower concentrations, *i.e.* 2.5 and 5 μM (Figure 6, panels A and B). The data indicate that only **4a** exerted a progressive reduction of cell viability. Indeed, after 48-h incubation, the cell growth was significantly reduced in the presence of 5 μM **4a** and, after 72-h treatment, the reduction of cell viability was significant even at 2.5 μM (Figure 6B). We have

then evaluated if compound **4a** exerted a cytotoxic effect even in normal cells, such as the non-malignant human fibroblast cell line BJ-5ta (Figure 6C). The MTT assay, performed at different concentrations and prolonged up to 72 h, clearly indicates that compound **4a** was not cytotoxic for this non-tumor cell line, even when present at 10 μM. It is known that fibroblasts are consistently and ubiquitously present in any body tissue; interestingly, the lack of cytotoxicity of **4a** in BJ-5ta suggests that this compound could not cause unspecific side-toxic effects in a normal cellular context.

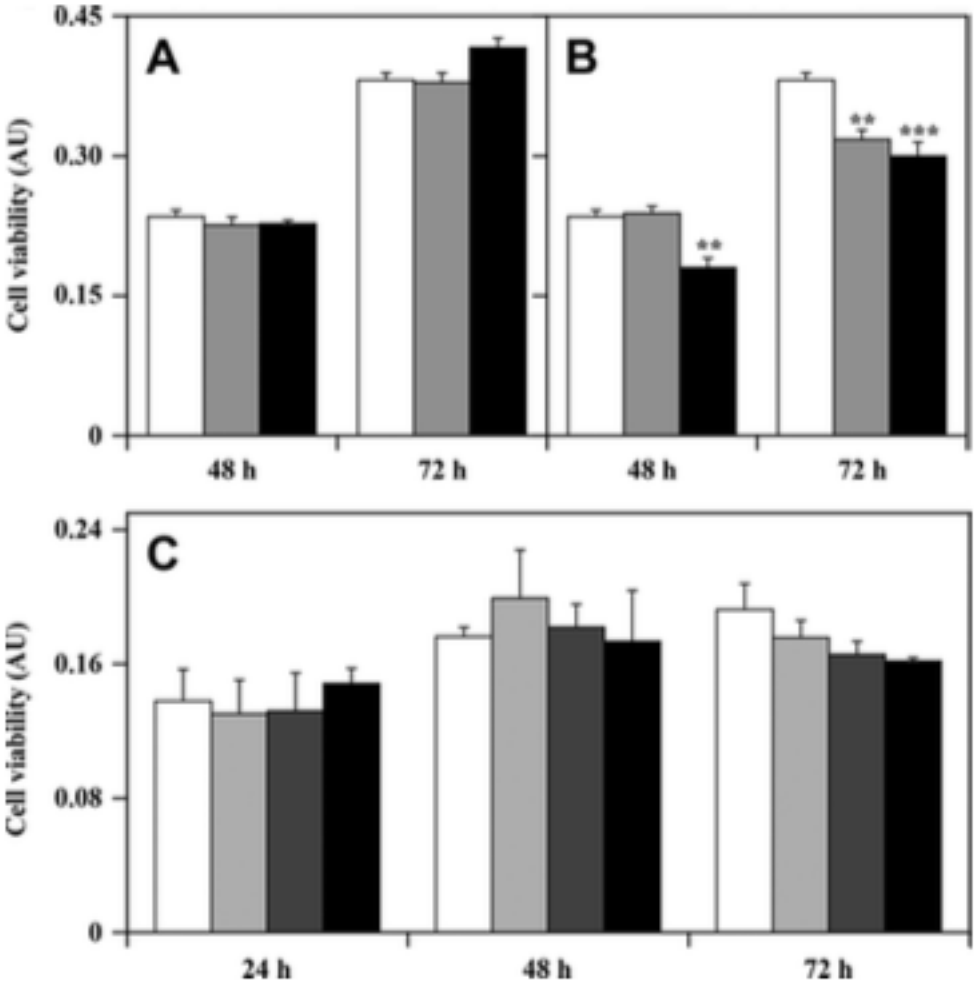

Figure 6. Cell toxicity of NPA derivatives. Panels (A,B) A2058 cells were incubated for 48 or 72 h with 0.5% (v/v) DMSO (open bars), 2.5 μM (gray bars) or 5.0 μM (black bars) of compound **4** (panel A) or **4a** (panel B). Panel (C) BJ-5ta cells were incubated for 24, 48, or 72 h with 0.5% (v/v) DMSO (open bars), 2.5 μM (light gray bars), 5.0 μM (dark gray bars), or 10 μM (black bars) of compound **4a**. Data of cell viability were obtained from at least three independent experiments and expressed in arbitrary units, as the mean ± SE. **, $p < 0.01$; ***, $p < 0.001$ compared to control cells. Other details are in the Experimental Section.

The cytotoxic effect of **4a** in melanoma cells prompted us to extend the evaluation of its inhibition power towards the recombinant forms of CDC25A and -C, besides that of -B. Under this concern, the values of K_i determined for CDC25A and -C were 3.0 µM and 1.9 µM, respectively. These data indicate that 4a is active towards the three different forms of CDC25. In the light of all these observations, compound **4a** was chosen for further biological

studies to better investigate its cytotoxicity in melanoma cell lines. Notably, the melanoma, in its late stage, represents one of the most aggressive tumors, characterized by a low responsiveness to conventional anti-tumoral therapies.[63] Therefore, **4a** is particularly attractive as it is active at low concentrations in melanoma cells. Under this concern, we should point out that the biological activity of the initial lead NSC28620 was observed only at much higher doses, *i.e.* 200 μM, and in more responsive tumor cell lines.[38]

To evaluate the long-term cell growth inhibitory effect, we determined if **4a** could suppress colony formation of melanoma cells. To this aim, A2058 and A375 melanoma cell lines were exposed to increasing concentrations of **4a** (0-10 μM) and colony formation was monitored. As shown in Figure 7, **4a** affected colony formation in a progressive and remarkable manner. Indeed, the number of cell clones progressively decreased with 0.625, 1.25 and 2.5 μM **4a** and was almost absent in the presence of 5 or 10 μM inhibitor in both cell lines. Hence, the capability to form cell clones, an intrinsic characteristic of tumors cells,[64] was reduced when melanoma cells were treated with very low concentration of **4a**.

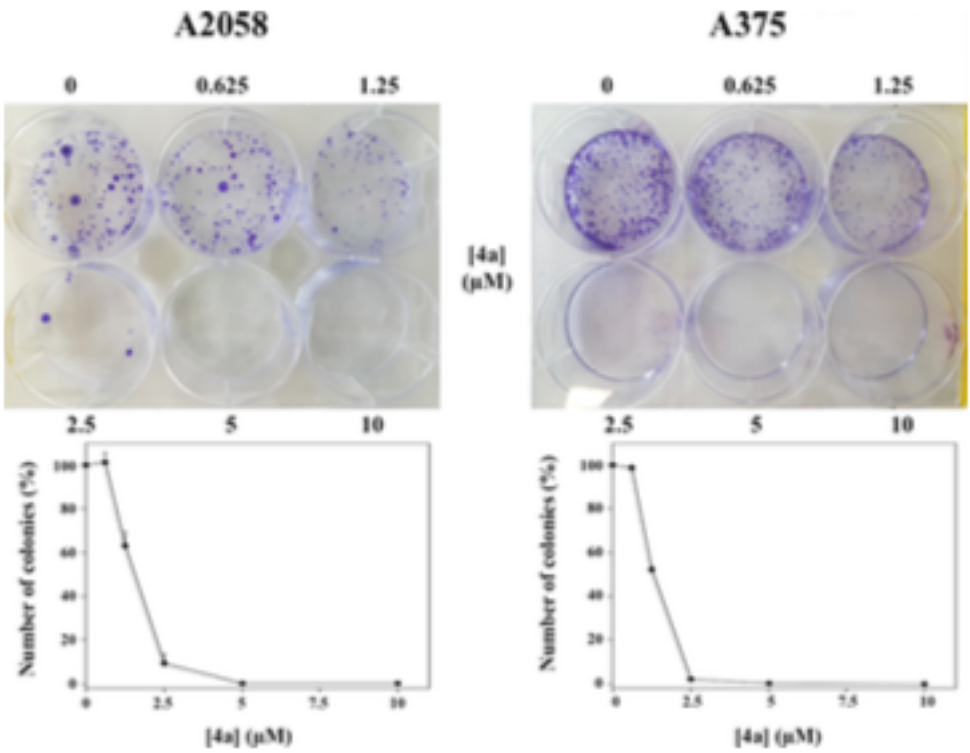

Figure 7. Effect of **4a** on the colony formation of melanoma cells. A2058 and A375 cells were treated with vehicle alone or 0.625, 1.25, 2.5, 5.0, or 10 μM **4a**. After 10 days treatment, plates were photographed and images of representative experiments are shown. The bottom plots report the number of colonies counted as indicated in the Experimental Section; values are expressed in percentages and reported as the mean ± SE from at least three different experiments.

Effect of 4a on Cell Cycle Progression and p-Cdk1. A further investigation on the mechanisms mediating the toxic action of **4a** in melanoma cells was carried out. It is noteworthy that CDC25 enzymes play a pivotal role in the regulation of cell cycle, as well as in the control of DNA damage.[15] Hence, the inhibitory potential of **4a** towards the CDC25B phosphatase activity suggests that this compound could lead to a cell cycle arrest in cultured cells. To evaluate the effect of **4a** on cell cycle progression, melanoma cells were exposed to 10 μM **4a** for 8- and 16-h and the cell cycle phase distribution was cytofluorimetrically monitored after PI staining for either A2058 (Figure 8) or A375 (Figure 9) cells. Compared to untreated cells, a significant increase of the G2/M phase associated to a reduction of G0/G1 phase was detected after 8-h treatment with **4a** in both A2058 (Figure 8A) and A375 (Figure

9A) cells. When the incubation was prolonged up to 16-h, a somehow different response emerged from the two cell lines. In A2058 cells, a further increase of cell percentage arrested in G2/M was evident, as well as an ulterior decrease of cells in G0/G1 phase, together with a small not-significant increase of the sub G1 phase (Figure 8B). On the other hand, in A375 cell lines the number of cells arrested in G2/M phase was similar between treated and untreated cells, the reduction of cell in G0/G1 phase was still evident but less pronounced compared to 8 h treatment, but interestingly, the increase of sub G1 phase became greatly significant, compared to untreated cells (Figure 9B). These results could indicate that the arrest in G2/M represents a cellular response to the toxic effect of **4a**, perhaps mediated by the CDC25 inhibition; however, this effect could evolve in cell death after a prolonged treatment, as suggested by the behavior of A375 cells. The significant increase of a sub G1 phase observed in A375 melanoma cells after 16-h treatment is probably due to the derivation of this cell line from a primary tumor, whereas A2058 is a metastatic tumor cell line; this different histological origin could explain the greater responsiveness of A375 cells to the drug treatment.

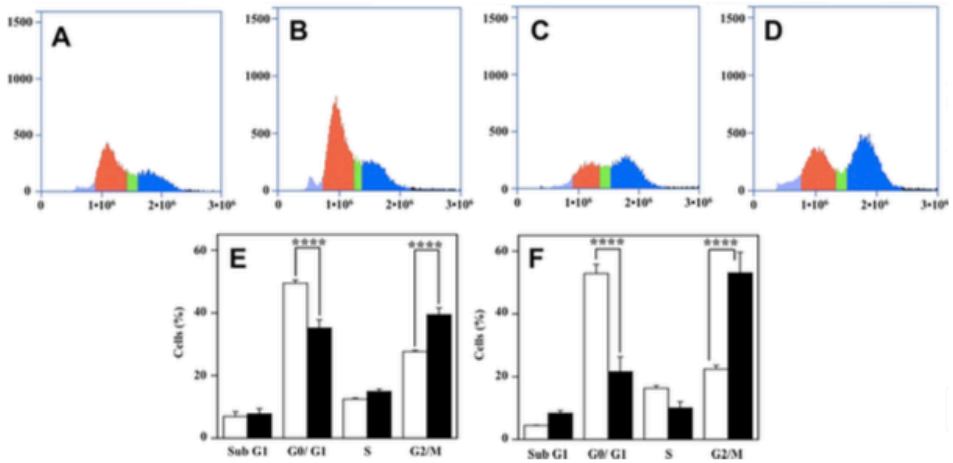

Figure 8. Effect of **4a** on the distribution of cell cycle phases of A2058 cells. The distribution of cells in the different phases was evaluated after 8 h (panels A,C) or 16 h (panels B,D) from treatment with 0.5% DMSO (panels A,B) or 10 μM **4a** (panels C,D) as described in the Experimental Section. Cell cycle phases colours: sub G1, light blue; G0/G1, red; S, green; G2/M, dark blue. Histograms show the cell percentage distribution among the various phases after 8 h (panel E) or 16 h (panel F). Data obtained from triplicate experiments in the presence of DMSO (open bars) or **4a** (black bars) are reported as the mean ± SE. ****, $p < 0.0001$ compared to control cells.

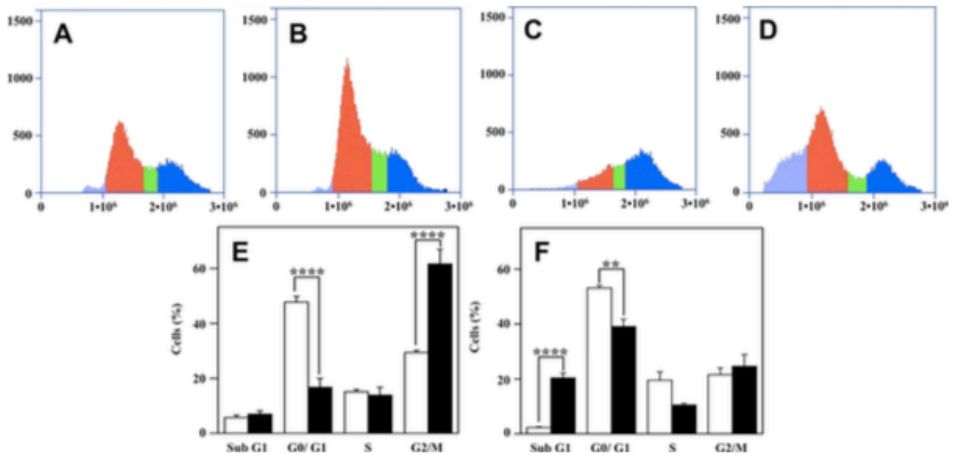

Figure 9. Effect of **4a** on the distribution of cell cycle phases of A375 cells. The same protocol described in the legend to Figure 8 was followed for analyzing the cell phases distribution of A375 cells. **, $p < 0.01$; ****, $p < 0.0001$ compared to control cells.

The arrest in G2/M of both melanoma cell lines during treatment with **4a** could be related to the inhibitory capacity of this molecule toward CDC25 phosphatase activity also in a cellular system. It is known that CDC25 enzymes regulate cell cycle progression by modulating the activity of Cdks, which represent their main targets.[65, 66] In particular, the phosphorylation of different substrates by Cdk1 is responsible for the modulation of many biochemical events involved in the entry to mitosis. Under this concern, a critical event for the activation of Cdk1 is the dephosphorylation of its inactive form, p-Cdk1, mediated by CDC25.[67-69] Therefore, we verified if the treatment of melanoma cells with **4a** could affect the protein levels of p-Cdk1. Indeed, as shown in Figure 10, an increase of p-Cdk1 became

evident in both melanoma cell lines after a short incubation time (8 h) with **4a**. Hence, the higher protein levels of p-Cdk1 found in melanoma with respect to untreated cells could represent a further evidence of the inhibitory effect exerted by **4a** on CDC25 enzymatic activity in these cellular systems.

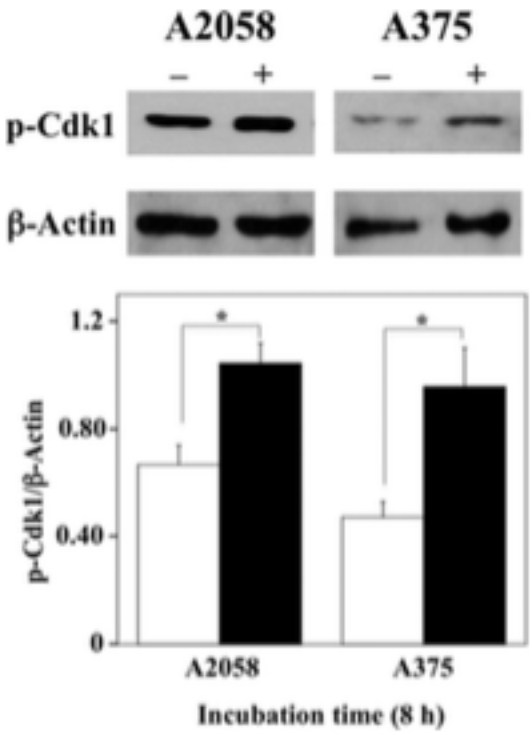

Figure 10. Effect of **4a** on p-Cdk1 protein levels. A2058 and A375 cells were incubated in the absence or in the presence of 10 μM **4a** for 8 h and total protein extracts were used to detect p-Cdk1 levels through western blot. β-Actin was used as an internal loading control. *, $p < 0.05$ compared to control cells.

CONCLUSIONS

Over the last years, many efforts have been devoted to the discovery of CDC25 inhibitors featuring novel chemotypes; however, only a limited number of literature reports have described the identification of inhibitors based on non-quinoid structures, although these compounds could be more attracting because intrinsically endowed with lower side-toxic effects.

In the present study we described the design, the synthesis, the inhibition mechanism, as well as the biological effects of novel NPK and NPA derivatives as inhibitors of CDC25B, that

were designed starting from the lead compound NSC28620, recently reported by us. Different synthetic pathways allowed the exploration of the effects of various substituents on the naphthalene moiety, as well as the role of the carboxylic function, leading to the identification of the main structural requirements for the inhibitory activity. Interestingly, the structural modifications had a profound impact on the inhibition mechanism: indeed, while the lead compound NSC28620 showed a competitive inhibition, the newly designed inhibitors displayed a non-competitive, or un-competitive, or mixed behavior. Some derivatives (**7j**, **7i**, **6e**, **7f** and **3**) showed higher inhibitory activity than the initial lead NSC28620, with the most potent inhibitor **7j** being 7-fold more active (K_i of 0.8 μM). IFD simulations helped to rationalize the molecular basis of the activity of this series of derivatives, which bind within the swimming pool pocket, as also demonstrated by kinetic analysis and intrinsic fluorescence studies. Moreover, the interaction of the carboxylic acid moiety of **7j** and its congeners with the key residues R482 and R544 accounts for the increased inhibitory potency towards CDC25B. On the other hand, the un-competitive derivatives, such as **3**, tightly fit in the hydrophobic cleft formed by the substrate OMFP and the swimming pool. These compounds were characterized for their cellular activity in the highly aggressive human melanoma cell lines A2058 and A375. In particular, compound **4a** was the most effective one in the inhibition of cell proliferation and colony formation, also causing an increase of the G2/M phase and a reduction of G0/G1 phase of the cell cycle in both cell lines. Importantly, **4a** induced an increase of p-Cdk1, providing a further evidence of the inhibitory effect on CDC25B. Furthermore, it is important to note that this compound exhibits a cytotoxic effect at low concentration in melanoma cells, an important issue for the possible reduction of undesired side effects. Our findings not only demonstrate the feasibility of exploiting CDC25s as a therapeutic target for melanoma, but also suggest that the NPA

scaffold represents an attractive starting point for further structural elaboration to achieve higher affinity, and more specific inhibition.

EXPERIMENTAL SECTION

Reagents and Chemicals. Reagents and solvents were purchased from Sigma-Aldrich and used without further purification. Some reactions involving air-sensitive reagents were performed under nitrogen atmosphere and anhydrous solvents were used when necessary. The Biotage Initiator 2.0 microwave synthesizer was used. Reactions were monitored by thin layer chromatography analysis on aluminum-backed Silica Gel 60 plates (70-230 mesh, Merck), using an ultraviolet fluorescent lamp at 254 nm and 365 nm. Visualization was aided by opportune staining reagents. Purification of intermediates and the final compounds was performed by flash chromatography using Geduran® Si 60 (40-63 μm, Merck). ^{1}H- and ^{13}C-NMR spectra were recorded at room temperature on a Varian Oxford 300 MHz instrument using TMS as internal standard. $CDCl_3$, CD_3OD, acetone-d_6 and DMSO-d_6 were used as deuterated solvents for all the spectra run. Chemical shift are expressed as δ (ppm). Multiplicity is reported as *s* (singlet), *br s* (broadened singlet), *d* (doublet), *t* (triplet), *q* (quartet), *m* (multiplet), *dd* (doublet of doublets), *dt* (doublet of triplets). The coupling constants (*J*-values) are given in Hertz (Hz). All spectroscopic data match the assigned structures. The melting points were determined on a Buchi Melting Point B540 instrument. MS analyses were carried out with a Thermo Finnigan LCQ Advantage system, equipped with a quaternary pump, a Diode Array Detector (working wavelength: 254 nm) and a MS spectrometer, with an Electrospray ionization source and an Ion Trap mass analyzer (ionization: ESI positive or ESI negative; capillary temperature: 250°C; source voltage: 5.50 kV; source current: 4.00 μA; multipole 1 and 2 offset: -5.50 V and -7.50 V, respectively; intermultipole lens voltage: -16.00 V; trap DC offset voltage: -10.00 V). Elemental analyses (CHN) are within ± 0.40% of theoretical values. The results of elemental analyses, carried out with a EurovectorEuro EA 3000 model analyzer, indicated that the purity of all tested compounds was higher than 95%.

General Procedure A. To a stirred mixture of the proper lactone (0.172 mmol) in 25% KOH (1 mL) and pyridine (0.5 mL), powdered $KMnO_4$ (43.5 mg, 0.275 mmol) was added, and the mixture was heated at reflux for 5 hours. The hot mixture was filtered and the residue was washed with water. Then, the filtrate was extracted with diethyl ether (2×2 mL) to remove the unreacted lactone. The aqueous phase was acidified with 3N HCl (2 mL), extracted with ethyl acetate (3×2 mL), washed with water and the organic layer was dried over anhydrous sodium sulfate. The organic solvent was evaporated under *vacuum* to give a crude oil, which was purified by flash chromatography eluting firstly with cyclohexane/ethyl acetate (80:20) and then (10:90) to afford the desired compounds.

General Procedure B. To a solution of the suitable bromobenzoic acid (2.487 mmol) in ethanol (1 mL), a catalytic amount of concentrated sulfuric acid was added dropwise. The resulting mixture was kept under stirring at reflux overnight and, after cooling, the solvent was evaporated under *vacuum*. Ethyl acetate (3 mL) was added, and the organic layer was firstly washed with a saturated solution of sodium bicarbonate (1×2 mL) and then with water (2×2 mL). The organic solvent was dried over anhydrous sodium sulfate and evaporated. Purification with flash chromatography (eluent: cyclohexane/ethyl acetate 90:10) was performed.[52]

General Procedure C. *Procedure C1*. A dried flask was purged with argon, charged with (±)-BINAP (3% mmol), and then toluene (2.7 mL) was added. The mixture was heated to 80°C under stirring until the BINAP was dissolved. The solution was cooled to room temperature, and $Pd(OAc)_2$ (2% mmol) was added. The mixture was stirred at room temperature for 1 minute, then a solution of the proper 1-bromonaphthalene (1.0 mmol) and the corresponding ethyl aminobenzoate (0.8 mmol) in toluene (0.5 mL) was added. Finally, Cs_2CO_3 (1.14 mmol) and other toluene (2 mL) were added to the reaction mixture. The solution was heated at 80°C under stirring; then, it was cooled to room temperature, diluted

with diethyl ether, filtered and concentrated. The obtained crude product was purified by column chromatography to provide the desired adduct.[49]

Procedure C2. A dried flask was purged with argon, charged with (±)-BINAP (3% mmol), and then toluene (2.7 mL) was added. The mixture was heated to 80°C under stirring until the BINAP was dissolved. The solution was cooled to room temperature, and $Pd(OAc)_2$ (2% mmol) was added. After stirring the mixture at room temperature for 1 minute, a solution of the suitable ethyl bromobenzoate (1.0 mmol) with the appropriate naphthylamine (0.8 mmol) in toluene (0.5 mL) was added. Cs_2CO_3 (1.14 mmol) was introduced within the mixture and toluene (2 mL) was added. The mixture was heated to 80°C under stirring; then, it was cooled to room temperature, diluted with diethyl ether, filtered, and concentrated. The crude product was purified by column chromatography to obtain the desired adduct.[49]

General Procedure D. To a solution of the suitable ethyl-(naphthylamino)-benzoate (0.15 mmol) in 2 mL of THF/EtOH (1:1), 1M NaOH (0.375 mmol) was added. The resulting mixture was refluxed for a different period of time, depending on the substrate. The solvent was evaporated, and then water (2 mL) was added. The aqueous phase was firstly washed with diethyl ether in order to purify the reaction mixture from the unreacted starting material, and then treated with 1N HCl (0.5 mL). The acid was extracted with ethyl acetate (3×1 mL), the organic phase was dried over anhydrous sodium sulfate and the solvent was evaporated under reduced pressure. The crude product was purified by flash chromatography eluting with dichloromethane/methanol (95:5) to afford the desired derivatives.[50]

General Procedure E. To a solution of the proper methoxynaphthalene (0.180 mmol) in dry dichloromethane (2 mL), BBr_3 (1M in dichloromethane, 0.945 mmol) was added dropwise under N_2. The reaction was carried out at room temperature for all the synthesized compounds. The starting solution was firstly cooled at -78°C and BBr_3 was carefully added dropwise to the reaction mixture. After 20 minutes, the resulting solution was warmed to

room temperature and the stirring was continued for further 3 hours. The reaction was then quenched at 0°C with water (4 mL), and extracted with ethyl acetate (3×2 mL). The combined organic phases were washed with brine (3×1 mL) and dried over anhydrous sodium sulfate. The subsequent filtration and evaporation of the organic solvent provided a crude product, which was purified by flash chromatography eluting firstly with dichloromethane/methanol (95:5) and then with dichloromethane/ methanol (80:20) to afford the final naphthol.[49]

General Procedures F. *Procedure F1*. To an ice-cold solution of the proper *tert*-butyl-naphthylcarbamate (1.67 mmol) in dry 1,4-dioxane (1 mL), HCl (4M in 1,4-dioxane, 1 mL) was added dropwise, under N_2. The reaction was stirred at room temperature for 24 hours. After completion of the reaction, monitored by TLC, diethyl ether was added to the reaction mixture and it was stirred. After cooling at 0°C, the formed precipitate was collected by filtration, washed with cold diethyl ether and dried to afford the hydrochloride salt of compound **7i** or **7j**.

Procedure F2. Trifluoroacetic acid (0.65 mmol) was added to a solution of the suitable *tert*-butyl-naphthylcarbamate (0.13 mmol) in dichloromethane (1 mL) and the reaction was stirred at room temperature for 60 min. The solvent was removed *in vacuo*; then, a 2M sodium hydroxide solution (2 mL) was added and extracted with ethyl acetate (3×1 mL). The organic layers were dried over anhydrous sodium sulfate and the solvent was evaporated under reduced pressure. Products **10** and **11** were isolated as hydrochloride salts by treatment with 1.25 M HCl in methanol.

General Procedure G. To a solution of the opportune benzoic acid (2.487 mmol) in ethanol (1 mL), a catalytic amount of concentrated sulfuric acid was added dropwise. The resulting mixture was stirred under microwave irradiation for 90 min at 80°C, and then the solvent was evaporated under reduced pressure. Ethyl acetate (3 mL) was added, and the

organic layer was firstly washed with a saturated solution of sodium bicarbonate (1×2 mL) and then with water (2×2 mL). The organic solvent was dried over anhydrous sodium sulfate and evaporated under *vacuum*. The crude product was purified by flash chromatography.[52]

General Procedure H. To a solution of the required bromonaphthol (0.672 mmol) in dry *N*,*N*-dimethylformamide (1 mL) sodium hydride (60% dispersion in mineral oil, 29.6 mg, 0.739 mmol) was added under N_2. After the evolution of H_2, iodomethane (0.17 mL, 2.688 mmol) was added, and the reaction mixture was stirred at room temperature for 3 hours. After the evaporation of *N*,*N*-dimethylformamide, the resulting residue was extracted with ethyl acetate (3×2 mL). The collected organic phase was dried over anhydrous sodium sulfate and the solvent was evaporated under reduced pressure to give the desired derivatives. The crude oils were purified by flash chromatography (cyclohexane/ethyl acetate 90:10) to provide compounds **16a** and **16b**.

General Procedure I. To a solution of the proper bromomethoxynaphthalene (0.422 mmol) in anhydrous THF (4 mL) cooled to -78°C under N_2 was added *n*-BuLi (2.7M in heptane, 0.39 mL, 1.055 mmol) and the resulting mixture was stirred for 1 hour. Anhydrous *N*,*N*-dimethylformamide (0.20 mL, 2.532 mmol) was added, and the reaction was stirred for a further 1 hour at -78°C. The reaction was quenched by a slow addition of cold water (0.5 mL), in order to neutralize the unreacted *n*-BuLi, and THF and DMF were evaporated. The residue was poured into 3N HCl (3 mL) and extracted with diethyl ether (6×2 mL). The combined organic layers were washed firstly with water, then with a saturated sodium hydrogen carbonate solution and, finally, with a saturated sodium chloride solution. The organic phase was dried, filtered and concentrated. The crude oils were purified by flash chromatography (cyclohexane/ethyl acetate 9:1) to provide compounds **17a** and **17b**.

General Procedure J. To a solution of compound **19** (0.787 mmol) in dry diethyl ether (1 mL) at -78°C was added dropwise 0.58 mL of a 2.7 M solution of *n*-BuLi in heptane

(1.574 mmol), under N_2, obtaining intermediate **20**. The solution was stirred at -78°C for 1 hour, then the suitable methoxy-1-naphthaldehyde (0.787 mmol) was added and the reaction mixture was stirred at room temperature overnight. To quench the unreacted *n*-BuLi, cold water (1 mL) was dropped in the reaction mixture and then the aqueous phase was extracted with ethyl acetate (3×2 mL). The organic phase was dried over anhydrous sodium sulfate and the solvent was evaporated under reduced pressure. The obtained oil (284.3 mg) was dissolved in a solution of 3N HCl (1.5 mL), and the mixture was heated at reflux for 4.5 hours. After cooling, the solid was collected and washed with water, in order to be taken up in aqueous 10% NaOH (1.5 mL) and heated at reflux for 1 hour. The product was collected upon acidification with 3N HCl (2 mL), extracted into ethyl acetate, washed with water and dried over anhydrous sodium sulfate. The solvent was evaporated under reduced pressure to give a crude solid, which was purified by flash chromatography eluting with cyclohexane/ethyl acetate (80:20).[48]

General Procedure K. To a solution of the suitable 1-nitronaphthalene (1.155 mmol) and triethylsilane (0.74 mL, 4.633 mmol) in ethanol (5 mL) a catalytic amount of palladium (II) chloride (10 mol %) was added under an N_2 atmosphere. The resulting mixture was kept under stirring and a change of color was observed. The solvent was evaporated and then water was added and decanted. The aqueous phase was extracted with diethyl ether (3×2 mL). The organic phase was firstly treated with 3N HCl (2 mL) and then the collected acidic aqueous solution, containing the hydrochloride salt of the naphthylamine, was basified with 25% NaOH (2 mL) and extracted with diethyl ether (6×2 mL). The organic phase was dried over anhydrous sodium sulfate and the solvent was evaporated under reduced pressure.[47]

General Procedure L. To a solution of the proper bromo-1-naphthalenamine (1.351 mmol) in ethanol (2.5 mL) di-*tert*-butyl dicarbonate (442.3 mg, 2.026 mmol) was added. The resulting mixture was kept under stirring for 24 hours at 30°C. Then, the solvent was

evaporated under reduced pressure and the crude oil was purified by flash chromatography, eluting with cyclohexane/ethyl acetate (90:10) to afford the products.

Synthesis of 2-(1-naphthoyl)benzoic acid (1). A mixture of 1-bromonaphthalene (200 mg, 0.966 mmol), magnesium turnings (47 mg, 1.931 mmol), and a catalytic amount of iodine in dry THF (2 mL) was refluxed under N_2 until the formation of the Grignard reagent. The latter was added dropwise, under N_2, to a solution of phthalic anhydride (143.1 mg, 0.966 mmol) in dry THF (1.5 mL), and the resulting mixture was heated under reflux for 48 hours. The reaction mixture was quenched with 0.5 mL of a saturated aqueous solution of ammonium chloride. The solvent was evaporated and then the aqueous layer was extracted with ethyl acetate (3×2 mL). In order to purify the reaction mixture from the unreacted starting material, the organic phase was firstly treated with a saturated solution of sodium bicarbonate (1 mL) and then the collected alkaline aqueous layer, which contained the sodium salt of compound **1**, was acidified with 3N HCl and extracted with ethyl acetate (3×2 mL). The organic phase was dried over anhydrous sodium sulfate, filtered, and the solvent was evaporated under reduced pressure. The crude oil was purified by flash chromatography eluting firstly with cyclohexane/ethyl acetate (80:20) and then with dichloromethane/methanol (95:5) to afford compound **1**. Pale green solid, m.p. 175-176°C, 73% yield. Molecular formula: $C_{18}H_{12}O_3$. Molecular Weight: 276.29 g/mol. Rf = 0.28 (dichloromethane/methanol 95:5). ^{1}H NMR (300 MHz, CD_3OD) δ 8.94 (d, *J* = 8.1 Hz, 1H, ArH), 7.98 (d, *J* = 8.1 Hz, 1H, ArH), 7.94-7.82 (m, 2H, ArH), 7.62-7.30 (m, 7H, ArH) ppm. ESI-MS (*m*/*z*) Calcd: 276 Found: 275 $[M-H]^-$. Anal. Calcd for $C_{18}H_{12}O_3$: C, 78.61; H, 4.86. Found: C, 78.45; H, 4.88.

2-(3-Methoxy-1-naphthoyl)benzoic acid (1a). Procedure A: starting from **21a**. White solid, m.p. 167-168°C, 71 % yield. Molecular formula: $C_{19}H_{14}O_4$. Molecular Weight: 306.31 g/mol. Rf = 0.31 (dichloromethane/methanol 95:5). ^{1}H NMR (300 MHz, CD_3OD) δ 8.81 (d, *J*

= 8.5 Hz, 1H, ArH), 7.89 (dd, J_1 = 7.0 Hz, J_2 = 2.0 Hz, 1H, ArH), 7.80 (d, J = 8.5 Hz, 1H, ArH), 7.60-7.40 (m, 6H, ArH), 6.99 (d, J = 2.0 Hz, 1H, ArH), 3.82 (s, 3H, CH_3) ppm. ESI-MS (*m*/*z*) Calcd: 306 Found: 305 $[M-H]^-$. Anal. Calcd for $C_{19}H_{14}O_4$: C, 74.50; H, 4.61. Found: C, 74.36; H, 4.63.

2-(4-Methoxy-1-naphthoyl)benzoic acid (1b). Procedure A: starting from **21b**. Brown solid, m.p. 196-197°C, 36 % yield. Molecular formula: $C_{19}H_{14}O_4$. Molecular Weight: 306.31 g/mol. Rf = 0.20 (dichloromethane/methanol 95:5). ^{1}H NMR (300 MHz, CD_3OD) δ 9.12 (d, J = 8.5 Hz, 1H, ArH), 8.28 (d, J = 8.5 Hz, 1H, ArH), 7.90-7.87 (m, 1H, ArH), 7.62 (dt, J_1 = 7.2 Hz, J_2 = 1.5 Hz, 1H, ArH), 7.54-7.45 (m, 4H, ArH), 7.39-7.36 (m, 1H, ArH), 6.76 (d, J = 8.1 Hz, 1H, ArH), 4.02 (s, 3H, CH_3) ppm. ESI-MS (*m*/*z*) Calcd: 306 Found: 305 $[M-H]^-$. Anal. Calcd for $C_{19}H_{14}O_4$: C, 74.50; H, 4.61 Found: C, 74.39; H, 4.59.

2-(3-Hydroxy-1-naphthoyl)benzoic acid (1c). Procedure E: starting from **1a**. Reaction time: 60 min. Foam, 6 % yield. Molecular formula: $C_{18}H_{12}O_4$. Molecular Weight: 292.29 g/mol. Rf = 0.10 (dichloromethane/methanol 95:5). ^{1}H NMR (300 MHz, CD_3OD) δ 8.78 (d, J = 8.1 Hz, 1H, ArH), 8.01 (dd, J_1 = 7.5 Hz, J_2 = 1.2 Hz, 1H, ArH), 7.72-7.64 (m, 3H, ArH), 7.53-7.37 (m, 3H, ArH), 7.28 (d, J = 2.6 Hz, 1H, ArH), 7.00 (d, J = 2.7 Hz, 1H, ArH) ppm. ESI-MS (*m*/*z*) Calcd: 292 Found: 291 $[M-H]^-$. Anal. Calcd for $C_{18}H_{12}O_4$: C, 73.97; H, 4.14. Found: C, 73.81; H, 4.12.

Ethyl 2-(2-naphthoyl)benzoate (2). Procedure B: starting from **1**. Yellow oil, 60 % yield. Molecular formula: $C_{20}H_{16}O_3$. Molecular Weight: 304.34 g/mol. Rf = 0.38 (cyclohexane/ethyl acetate 90:10). ^{1}H NMR (300 MHz, $CDCl_3$) δ 9.07 (d, J = 8.4 Hz, 1H, ArH), 8.0-7.97 (m, 2H, ArH), 7.90 (d, J = 8.4 Hz, 1H, ArH), 7.60-7.50 (m, 5H, ArH), 7.45 (d, J = 7.5 Hz, 1H, ArH), 7.36 (t, J = 8.4 Hz, 1H, ArH), 3.90 (q, J = 7.2 Hz, 2H, CH_2), 0.91 (t, J = 7.2 Hz, 3H, CH_3) ppm. ESI-MS (*m*/*z*) Calcd: 304 Found: 303 $[M-H]^-$. Anal. Calcd for $C_{20}H_{16}O_3$: C, 78.93; H, 5.30; Found: C, 78.81; H, 5.35.

Ethyl 2-(naphthalen-1-ylamino)benzoate (3). Procedure C1: starting from 1-bromonaphthalene and ethyl-2-amino-benzoate. Reaction time: 17 hours. Silver foam, quantitative yield. Molecular formula: $C_{19}H_{17}NO_2$. Molecular Weight: 291.34 g/mol. Rf = 0.47 (cyclohexane/ethyl acetate 98:2). Eluent for chromatography: firstly only cyclohexane, then cyclohexane/ ethyl acetate from (98:2) to till (90:10). ^{1}H NMR (300 MHz, $CDCl_3$) δ 9.85 (br s, 1H, NH, exchangeable with D_2O), 8.13-8.10 (m, 1H, ArH), 8.05 (dd, J_1 = 7.8 Hz, J_2 = 1.2 Hz 1H, ArH), 7.91-7.88 (m, 1H, ArH), 7.71 (d, J = 7.8 Hz, 1H, ArH), 7.55-7.45 (m, 4H, ArH), 7.27-7.22 (m, 1H, ArH), 6.96 (dd, J_1 = 8.7 Hz, J_2 = 0.9 Hz, 1H, ArH), 6.73 (dt, J_1 = 7.8 Hz, J_2 = 1.2 Hz, 1H, ArH), 4.43 (q, J = 7.2 Hz, 2H, CH_2), 1.45 (t, J = 7.2 Hz, 3H, CH_3) ppm. ESI-MS (*m*/*z*) Calcd: 291 Found: 290 $[M-H]^-$. Anal. Calcd for $C_{19}H_{17}NO_2$: C, 78.33; H, 5.88; N, 4.81. Found: C, 78.78; H, 5.87; N, 4.79.

Ethyl-2-(3-methoxy-1-naphthylamino)benzoate (3a). Procedure C1: starting from 1-bromo-3-methoxynaphthalene (**16a**) and ethyl-2-aminobenzoate. Reaction time: 18 hours. Yellow oil, 71% yield. Molecular formula: $C_{20}H_{19}NO_3$. Molecular Weight: 321.37 g/mol. Rf = 0.62 (cyclohexane/ethyl acetate 90:10). Eluent for chromatography: cyclohexane/ethyl acetate (90:10). ^{1}H NMR (300 MHz, $CDCl_3$) δ 9.98 (br s, 1H, NH, exchangeable with D_2O), 8.08 (d, J = 8.1 Hz, 2H, ArH), 7.79 (d, J = 8.1 Hz, 1H, ArH), 7.50 (t, J = 8.1 Hz, 1H, ArH), 7.41-7.28 (m, 3H, ArH), 7.19 (d, J = 8.4 Hz, 1H, ArH), 7.02 (d, J = 2.4 Hz, 1H, ArH), 6.79 (t, J = 7.8 Hz, 1H, ArH), 4.45 (q, J = 6.9 Hz, 2H, CH_2), 3.95 (s, 3H, OCH_3), 1.47 (t, J = 6.9 Hz, 3H, CH_3) ppm. ESI-MS (*m*/*z*) Calcd: 321 Found: 320 $[M-H]^-$. Anal. Calcd for $C_{20}H_{19}NO_3$: C, 74.75; H, 5.96; N, 4.36. Found: C, 74.61; H, 5.94; N, 4.38.

Ethyl-2-(4-methoxy-1-naphthylamino)benzoate (3b). Procedure C2: starting from 1-amino-4-methoxynaphthalene (**25**) and ethyl-2-bromobenzoate (**22**). Reaction time: 18 hours. Yellow oil, 98% yield. Molecular formula: $C_{20}H_{19}NO_3$. Molecular Weight: 321.37 g/mol. Rf = 0.40 (cyclohexane/ethyl acetate 98:2). Eluent for chromatography: cyclohexane/ethyl

acetate (98:2). ^{1}H NMR (300 MHz, $CDCl_3$) δ 9.49 (br s, 1H, NH, exchangeable with D_2O), 8.30 (d, *J* = 8.8 Hz, 1H, ArH), 8.06-7.89 (m, 2H, ArH), 7.55-7.42 (m, 2H, ArH), 7.37 (d, *J* = 8.2 Hz, 1H, ArH), 7.15 (t, *J* = 8.4 Hz, 1H, ArH), 6.82 (d, *J* = 8.3 Hz, 1H, ArH), 6.67-6,57 (m, 2H, ArH), 4.41 (q, *J* = 7.1 Hz, 2H, CH_2), 4.03 (s, 3H, OCH_3), 1.44 (t, *J* = 7.1 Hz, 3H, CH_3) ppm. ESI-MS (*m*/*z*) Calcd: 321 Found: 320 $[M-H]^-$. Anal. Calcd for $C_{20}H_{19}NO_3$: C, 74.75; H, 5.96; N, 4.36. Found: C, 74.63; H, 5.98; N, 4.31.

Ethyl 2-(5-methoxy-1-naphthylamino)benzoate (3c). Procedure C2: starting from 1-amino-5-methoxynaphthalene and ethyl-2-bromobenzoate (**22**). Reaction time: 18 hours. Yellow oil, 72.66% yield. Molecular formula: $C_{20}H_{19}NO_3$. Molecular Weight: 321.37 g/mol. Rf = 0.58 (cyclohexane/ethyl acetate 95:5). Eluent for chromatography: cyclohexane/ethyl acetate (95:5). ^{1}H NMR (300 MHz, $CDCl_3$) δ 9.80 (br s, 1H, NH exchangeable with D_2O), 8.13 (dd, J_1 = 8.5 Hz, J_2 = 0.8 Hz, 1H, ArH), 8.02 (dd, J_1 = 7.8 Hz, J_2 = 1.2 Hz, 1H, ArH), 7.67 (d, *J* = 8.5 Hz, 1H, ArH), 7.58-7.32 (m, 3H, ArH), 7.23-7.20 (m, 1H, ArH), 6.96-6.79 (m, 2H, ArH), 6.70 (t, *J* = 7.8 Hz, 1H, ArH), 4.41 (q, *J* = 7.1 Hz, 2H, CH_2), 4.02 (s, 3H, OCH_3), 1.44 (t, *J* = 7.1 Hz, 3H, CH_3).

Ethyl 2-(5-((*tert*-butoxycarbonyl)amino)-1-naphthylamino)benzoate (3h). Procedure C1: starting from *tert*-butyl (5-bromonaphthalen-1-yl)carbamate (**27**) and ethyl-2-aminobenzoate. Reaction time: 18 hours. Foam, 76% yield. Molecular formula: $C_{24}H_{26}N_2O_4$. Molecular Weight: 406.47 g/mol. Rf = 0.58 (cyclohexane/ethyl acetate 80:20). Eluent for chromatography: cyclohexane/ethyl acetate (80:20). ^{1}H NMR (300 MHz, $CDCl_3$) δ 9.84 (br s, 1H, NH exchangeable with D_2O), 8.03 (dd, J_1 = 7.9 Hz, J_2 = 1.2 Hz, 1H, ArH), 7.91 (dd, J_1 = 8.4 Hz, J_2 = 1.6 Hz, 1H, ArH), 7.72 (d, *J* = 7.9 Hz, 1H, ArH), 7.56-7.38 (m, 3H, ArH), 7.31-7.17 (m, 2H, ArH and NHCO exchangeable with D_2O), 7.00-6.79 (m, 2H, ArH), 6.73 (t, *J* = 7.5 Hz, 1H, ArH), 4.41 (q, *J* = 7.1 Hz, 2H, CH_2), 1.57 (s, 9H, CH_3), 1.44 (t, *J* = 7.1 Hz, 3H, CH_3).

Ethyl 3-(naphthalen-1-ylamino)benzoate (4). Procedure C1: starting from 1-bromonaphthalene and ethyl-3-aminobenzoate. Reaction time: 17 hours. Yellow-brown oil, 83% yield. Molecular formula: $C_{19}H_{17}NO_2$. Molecular Weight: 291.34 g/mol. Rf = 0.39 (cyclohexane/ethyl acetate 90:10). Eluent for chromatography: cyclohexane/ethyl acetate (95:5). ^{1}H NMR (300 MHz, $CDCl_3$) δ 8.01 (dd, J_1 = 8.4 Hz, J_2 = 1.2 Hz, 1H, ArH), 7.88 (dd, J_1 = 7.0 Hz, J_2 = 2.5 Hz, 1H, ArH), 7.71-7.67 (m, 1H, ArH), 7.64-7.36 (m, 6H, ArH), 7.28 (t, J = 8.1 Hz, 1H, ArH), 7.12 (dd, J_1 = 8.1 Hz, J_2 = 2.4 Hz, 1H, ArH), 6.06 (br s, 1H, NH, exchangeable with D_2O), 4.36 (q, J = 7.1 Hz, 2H, CH_2), 1.38 (t, J = 7.1 Hz, 3H, CH_3) ppm. ESI-MS (*m*/*z*) Calcd: 291 Found: 290 $[M-H]^-$. Anal. Calcd for $C_{19}H_{17}NO_2$: C, 78.33; H, 5.88; N, 4.81. Found: C, 78.35; H, 5.80; N, 4.79.

Ethyl-3-(3-methoxy-1-naphthylamino)benzoate (4a). Procedure C1: starting from 1-bromo-3-methoxynaphthalene (**16a**) and ethyl-3-aminobenzoate. Reaction time: 18 hours. Yellow oil, 85% yield. Molecular formula: $C_{20}H_{19}NO_3$. Molecular Weight: 321.37 g/mol. Rf = 0.36 (cyclohexane/ethyl acetate 90:10). Eluent for chromatography: cyclohexane/ethyl acetate (98:2). ^{1}H NMR (300 MHz, $CDCl_3$) δ 7.91 (d, J = 8.1 Hz, 1H, ArH), 7.78-7.74 (m, 2H, ArH), 7.63 (dt, J_1 = 7.5 Hz, J_2 = 1.2 Hz, 1H, ArH), 7.49- 744 (m, 1H, ArH), 7.36-7.21 (m, 3H, ArH), 7.04 (d, J = 2.4 Hz, 1H, ArH), 6.90 (d, J = 2.1 Hz, 1H, ArH), 6.13 (br s, 1H, NH, exchangeable with D_2O), 4.37 (q, J = 6.9 Hz, 2H, CH_2), 3.90 (s, 3H, OCH_3), 1.39 (t, J = 6.9 Hz, 3H, CH_3) ppm. ESI-MS (*m*/*z*) Calcd: 321 Found: 320 $[M-H]^-$. Anal. Calcd for $C_{20}H_{19}NO_3$: C, 74.75; H, 5.96; N, 4.36. Found: C, 74.62; H, 5.98; N, 4.32.

Ethyl-3-(4-methoxy-1-naphthylamino)benzoate (4b). Procedure C1: starting from 1-bromo-4-methoxynaphthalene (**16b**) and ethyl-3-aminobenzoate. Reaction time: 40 hours, 40% yield. Procedure C2: starting from 1-amino-4-methoxynaphthalene (**25**) and ethyl-3-bromobenzoate (**23**). Reaction time: 24 hours, 94% yield. Brown oil. Molecular formula: $C_{20}H_{19}NO_3$. Molecular Weight: 321.37 g/mol. Rf = 0.25 (cyclohexane/ethyl acetate 90:10).

Eluent for chromatography: cyclohexane/ethyl acetate (90:10). ^{1}H NMR (300 MHz, $CO(CD_3)_2$) δ 8.30-8.26 (m, 1H, ArH), 8.05-8.02 (m, 1H, ArH), 7.53-7.46 (m, 3H, ArH), 7.39-7.34 (m, 1H, NH, exchangeable with D_2O; 2H, ArH), 7.23 (t, *J* = 7.8 Hz, 1H, ArH), 7.00-6.95 (m, 2H, ArH), 4.28 (q, *J* = 7.1 Hz, 2H, CH_2), 4.05 (s, 3H, OCH_3), 1.31 (t, *J* = 7.1 Hz, 3H, CH_3) ppm. ESI-MS (*m*/*z*) Calcd: 321 Found: 320 $[M-H]^-$. Anal. Calcd for $C_{20}H_{19}NO_3$: C, 74.75; H, 5.96; N, 4.36. Found: C, 74.64; H, 5.93; N, 4.38.

Ethyl 3-(5-methoxy-1-naphthylamino)benzoate (4c). Procedure C2: starting from 1-amino-5-methoxynaphthalene and ethyl-3-bromobenzoate (**23**). Reaction time: 18 hours. Brown oil, 47% yield. Molecular formula: $C_{20}H_{19}NO_3$. Molecular Weight: 321.37 g/mol. Rf = 0.31 (cyclohexane/ethyl acetate 90:10). Eluent for chromatography: cyclohexane/ethyl acetate (90:10). ^{1}H NMR (300 MHz, $CDCl_3$) δ 8.05 (t, *J* = 4.8 Hz, 1H, ArH), 7.65 (s, 1H, ArH), 7.56 (t, *J* = 7.2 Hz, 1H, ArH), 7.44-7.36 (m, 3H, ArH, 1H, NH), 7.30-7.24 (m, 2H, ArH), 7.12-7.08 (m, 1H, ArH), 6.86 (d, *J* = 7.6 Hz,, 1H, ArH), 4.35 (q, *J* = 7.1 Hz, 2H, CH_2), 4.02 (s, 3H, OCH_3), 1.37 (t, *J* = 7.1 Hz, 3H, CH_3).

Ethyl-3-(4-((*tert*-butoxycarbonyl)amino)-1-naphthylamino)benzoate (4g). Procedure C1: starting from *tert*-butyl (4-bromonaphthalen-1yl)carbamate (**26**) and ethyl-3-aminobenzoate. Reaction time: 18 hours. Silver foam, 83% yield. Molecular formula: $C_{24}H_{26}N_2O_4$. Molecular Weight: 406.47 g/mol. Rf = 0.40 (cyclohexane/ethyl acetate 80:20). Eluent for chromatography: cyclohexane/ethyl acetate (80:20). ^{1}H NMR (300 MHz, CD_3OD) δ 8.09 (d, *J* = 8.1 Hz, 1H, ArH), 8.02 (d, *J* = 8.4 Hz, 1H, ArH), 7.57-7.41 (m, 5H, ArH), 7.34 (d, *J* = 8.1 Hz, 1H, ArH), 7.25 (t, *J* = 7.8 Hz, 1H, ArH), 7.11 (dd, J_1 = 8.1 Hz, J_2 = 2.1 Hz, 1H, ArH), 4.30 (q, *J* = 7.2 Hz, 2H, CH_2), 1.55 (s, 9H, CH_3), 1.34 (t, *J* = 7.2 Hz, 3H, CH_3) ppm.

Ethyl-3-(5-((*tert*-butoxycarbonyl)amino)-1-naphthylamino)benzoate (4h). Procedure C1: starting from *tert*-butyl (5-bromonaphthalen-1yl)carbamate (**27**) and ethyl-3-

aminobenzoate. Reaction time: 18 hours. Foam, 85% yield. Molecular formula: $C_{24}H_{26}N_2O_4$. Molecular Weight: 406.47 g/mol. Rf = 0.33 (cyclohexane/ethyl acetate 80:20). Eluent for chromatography: cyclohexane/ethyl acetate (80:20). ^{1}H NMR (300 MHz, $CDCl_3$) δ 7.82 (d, *J* = 7.5 Hz, 1H, ArH), 7.70 (d, *J* = 8.4 Hz, 1H, ArH), 7.59 (t, *J* = 1.8 Hz, 1H, ArH), 7.54-7.47 (m, 2H, ArH), 7.35-7.26 (m, 4H, ArH), 7.18 (t, *J* = 7.5 Hz, 1H, ArH), 7.02 (dd, J_1 = 8.4 Hz, J_2 = 1.5 Hz, 1H, ArH), 6.83 (br s, 1H, NH, exchangeable with D_2O), 6.02 (br s, 1H, NH, exchangeable with D_2O), 4.26 (q, *J* = 6.9 Hz, 2H, CH_2), 1.48 (s, 9H, CH_3), 1.28 (t, *J* = 6.9 Hz, 3H, CH_3) ppm.

1-(*N*-Phenylamino)naphthalene (5). Procedure C1: starting from 1-bromonaphthalene and aniline. Reaction time: 18 hours. Yellow-brown solid, m.p. 61-63°C, 34 % yield. Molecular formula: $C_{16}H_{13}N$. Molecular Weight: 219.28 g/mol. Rf = 0.58 (cyclohexane/ethyl acetate 90:10). Eluent for chromatography: firstly only cyclohexane and then cyclohexane/ ethyl acetate (95:5). ^{1}H NMR (300 MHz, $CDCl_3$) δ 8.04 (dd, J_1 = 7.2 Hz, J_2 = 2.1 Hz, 1H, ArH), 7.89 (dd, J_1 = 7.2 Hz, J_2 = 2.1 Hz, 1H, ArH), 7.59 (dd, J_1 = 7.2 Hz, J_2 = 2.1 Hz, 1H, ArH), 7.53-7.40 (m, 4H, ArH), 7.31-7.26 (m, 2H, ArH), 7.03-7.00 (m, 2H, ArH), 6.94 (t, J_1 = 7.2 Hz, J_2 = 1.2 Hz, 1H, ArH), 5.95 (br s, 1H, NH, exchangeable with D_2O) ppm. ESI-MS (*m*/*z*) Calcd: 219 Found: 218 $[M-H]^-$. Anal. Calcd for $C_{16}H_{13}N$: C, 87.64; H, 5.98; N, 6.39. Found: C, 87.54; H, 5.97; N, 6.36.

2-(Naphthalen-1-ylamino)benzoic acid (6). Procedure D: starting from **3**. Reaction time: 60 min. Yellow solid, m.p. 230°C, 98 % yield. Molecular formula: $C_{17}H_{13}NO_2$. Molecular Weight: 263.29 g/mol. Rf = 0.39 (dichloromethane/methanol 95:5). ^{1}H NMR (300 MHz, $CO(CD_3)_2$) δ 10.09 (br s, 1H, NH, exchangeable with D_2O), 8.09-8.07 (m, 2H, ArH), 7.97-7.95 (m, 1H, ArH), 7.77 (d, *J* = 7.5 Hz, 1H, ArH), 7.58-7.51 (m, 4H, ArH), 7.33 (t, *J* = 8.7 Hz, 1H, ArH), 6.97 (d, *J* = 8.7 Hz, 1H, ArH), 6.78 (t, *J* = 7.5 Hz, 1H, ArH) ppm. ESI-MS

(*m*/*z*) Calcd: 263 Found: 262 $[M-H]^-$. Anal. Calcd for $C_{17}H_{13}NO_2$: C, 77.55; H, 4.98; N, 5.32. Found: C, 77.46; H, 4.99; N, 5.29.

2-(3-Methoxy-1-naphthylamino)benzoic acid (6a). Procedure D: starting from **3a**. Reaction time: 30 min. Yellow foam, quantitative yield. Molecular formula: $C_{18}H_{15}NO_3$. Molecular Weight: 293.32 g/mol. Rf = 0.34 (dichloromethane/methanol 95:5). ^{1}H NMR (300 MHz, $CO(CD_3)_2$) δ 10.15 (br s, 1H, NH, exchangeable with D_2O), 7.96 (d, *J* = 8.4 Hz, 1H, ArH), 7.85 (d, *J* = 8.4 Hz, 1H, ArH), 7.71 (d, *J* = 8.1 Hz, 1H, ArH), 7.35 (t, *J* = 7.2 Hz, 1H, ArH), 7.24-7.20 (m, 2H, ArH), 7.08 (d, *J* = 2.1 Hz, 1H, ArH), 7.02-6.99 (m, 2H, ArH), 6.68 (d, *J* = 7.2 Hz, 1H, ArH), 3.80 (s, 3H, CH_3) ppm. ESI-MS (*m*/*z*) Calcd: 293 Found: 292 $[M-H]^-$. Anal. Calcd for $C_{18}H_{15}NO_3$: C, 73.71; H, 5.15; N, 4.78. Found: C, 73.57; H, 5.13; N, 4.76.

2-(4-Methoxy-1-naphthylamino)benzoic acid (6b). Procedure D: starting from **3b**. Reaction time: 90 min. Oil, 53 % yield. Molecular formula: $C_{18}H_{15}NO_3$. Molecular Weight: 293.32 g/mol. Rf = 0.54 (dichloromethane/methanol 95:5). ^{1}H NMR (300 MHz, $CO(CD_3)_2$) δ 9.72 (br s, 1H, NH, exchangeable with D_2O), 8.34-8.25 (m, 1H, ArH), 8.03 (dd, J_1 = 8.0 Hz, J_2 = 1.6 Hz, 1H, ArH), 7.96-7.89 (m, 1H, ArH), 7.58-7.48 (m, 2H, ArH), 7.44 (d, *J* = 8.1 Hz, 1H, ArH), 7.23 (dt, J_1 = 8.4 Hz, J_2 = 1.6 Hz, 1H, ArH), 7.01 (d, *J* = 8.1 Hz, 1H, ArH), 6.69 (t, *J* = 7.6 Hz, 1H, ArH), 6.58 (d, *J* = 8.5 Hz, 1H, ArH), 4.07 (s, 3H, CH_3) ppm. ESI-MS (*m*/*z*) Calcd: 293 Found: 292 $[M-H]^-$. Anal. Calcd for $C_{18}H_{15}NO_3$: C, 73.71; H, 5.15; N, 4.78. Found: C, 73.59; H, 5.13; N, 4.77.

2-(5-Methoxy-1-naphthylamino)benzoic acid (6c). Procedure D: starting from **3c**. Reaction time: 90 min. Solid, m.p. 203-205°C, 82% yield. Molecular formula: $C_{18}H_{15}NO_3$. Molecular Weight: 293.32 g/mol. Rf = 0.48 (dichloromethane/methanol 95:5). Eluent for chromatography: dichloromethane/methanol (95:5). ^{1}H NMR (300 MHz, $CDCl_3$) δ 9.58 (br s, 1H, NH, exchangeable with D_2O), 8.17 (d, *J* = 8.2 Hz, 1H, ArH), 8.04 (d, *J* = 8.2 Hz, 1H,

ArH), 7.64 (d, *J* = 8.5 Hz, 1H, ArH), 7.54-7.37 (m, 4H, ArH), 6.87-6.82 (m, 2H, ArH), 6.71 (t, *J* = 7.5 Hz, 1H, ArH), 4.03 (s, 3H, CH_3).

2-(3-Hydroxy-1-naphthylamino)benzoic acid (6d). Procedure E: starting from **6a**. Reaction time: 30 min. Brown-purple foam, 90% yield. Molecular formula: $C_{17}H_{13}NO_3$. Molecular Weight: 279.29 g/mol. Rf = 0.17 (dichloromethane/methanol 95:5). ^{1}H NMR (300 MHz, $CO(CD_3)_2$) δ 10.00 (br s, 1H, NH, exchangeable with D_2O), 7.95 (dd, J_1 = 7.8 Hz, J_2 = 1.5 Hz, 1H, ArH), 7.81 (d, *J* = 8.4 Hz, 1H, ArH), 7.59 (d, *J* = 7.8 Hz, 1H, ArH), 7.32-7.10 (m, 4H, ArH), 6.99 (d, *J* = 8.4 Hz, 1H, ArH), 6.93 (d, *J* = 1.8 Hz, 1H, ArH), 6.67 (t, *J* = 7.5 Hz, 1H, ArH) ppm. ESI-MS (*m*/*z*) Calcd: 279 Found: 278 $[M-H]^-$. Anal. Calcd for $C_{17}H_{13}NO_3$: C, 73.11; H, 4.69; N, 5.02. Found: C, 73.01; H, 4.71; N, 5.04.

2-(4-Hydroxy-1-naphthylamino)benzoic acid (6e). Procedure E: starting from **6b**. Reaction time: 2 h. Dark solid, m.p. 214-215°C, 98% yield. Molecular formula: $C_{17}H_{13}NO_3$. Molecular Weight: 279.30 g/mol. Rf = 0.18 (dichloromethane/methanol 95:5). Eluent for chromatography: dichloromethane/methanol (95:5). ^{1}H NMR (300 MHz, $CO(CD_3)_2$) δ 11.21 (br s, 1H, COOH, exchangeable with D_2O), 9.66 (br s, 1H, NH, exchangeable with D_2O), 9.13 (br s, 1H, OH, exchangeable with D_2O), 8.34-8.28 (m, 1H, ArH), 8.02 (dd, J_1= 8.1 Hz, J_2= 1.6 Hz, 1H, ArH), 7.92-7.85 (m, 1H, ArH,), 7.55-7.47 (m, 2H, ArH), 7.32 (d, *J* = 8.1 Hz, 1H, ArH), 7.21 (dt, J_1 = 8.5 Hz, J_2 = 1.5 Hz 1H, ArH), 6.98 (d, *J* = 8.1 Hz, 1H, ArH), 6.67 (t, *J* = 8.1 Hz, 1H, ArH), 6.54 (d, *J* = 8.5 Hz, 1H, ArH). ESI-MS (*m*/*z*) Calcd: 279 Found: 278 $[M-H]^-$. Anal. Calcd for $C_{17}H_{13}NO_3$: C, 73.11; H, 4.69; N, 5.02. Found: C, 73.15; H, 4.68; N, 5.04.

2-(5-Hydroxy-1-naphthylamino)benzoic acid (6f). Procedure E: starting from **6c**. Reaction time: 30 min. Green foam, 72 % yield. Molecular formula: $C_{17}H_{13}NO_3$. Molecular Weight: 279.29 g/mol. Rf = 0.30 (dichloromethane/methanol 95:5). ^{1}H NMR (300 MHz, $CO(CD_3)_2$) δ 10.05 (br s, 1H, COOH, exchangeable with D_2O), 8.13 (d, *J* = 8.3 Hz, 1H,

ArH), 8.06 (dd, J_1 = 8.0 Hz, J_2 = 1.6 Hz, 1H, ArH), 7.61-7.41 (m, 3H, ArH), 7.39-7.24 (m, 2H, ArH), 6.97 (d, J = 7.6 Hz, 2H, ArH), 6.76 (td, J_1 = 7.5 Hz, J_2 = 1.5 Hz, 1H, ArH). ESI-MS (*m*/*z*) Calcd: 279 Found: 278 $[M-H]^-$. Anal. Calcd for $C_{17}H_{13}NO_3$: C, 73.11; H, 4.69; N, 5.02. Found: C, 73.04; H, 4.71; N, 5.00.

3-(1-Naphthylamino)benzoic acid (7). Procedure D: starting from **4**. Reaction time: 60 min. Oil, 96 % yield. Molecular formula: $C_{17}H_{13}NO_2$. Molecular Weight: 263.29 g/mol. Rf = 0.25 (dichloromethane/methanol 95:5). ^{1}H NMR (300 MHz, CD_3OD) δ 8.12 (d, J = 7.5 Hz, 1H, ArH), 7.82 (d, J = 7.5 Hz, 1H, ArH), 7.64 (s, 1H, ArH), 7.52-7.32 (m, 6H, ArH), 7.20 (t, J = 7.5 Hz, 1H, ArH), 7.08 (d, J = 7.5 Hz, 1H, ArH) ppm. ESI-MS (*m*/*z*) Calcd: 263 Found: 262 $[M-H]^-$. Anal. Calcd for $C_{17}H_{13}NO_2$: C, 77.55; H, 4.98; N, 5.32. Found: C, 77.43; H, 4.96; N, 5.31.

3-(3-Methoxy-1-naphthylamino)benzoic acid (7a). Procedure D: starting from **4a**. Reaction time: 40 min. Oil, 96 % yield. Molecular formula: $C_{18}H_{15}NO_3$. Molecular Weight: 293.32 g/mol. Rf = 0.19 (dichloromethane/methanol 95:5). ^{1}H NMR (300 MHz, $CO(CD_3)_2$) δ 7.95 (d, J = 8.4 Hz, 1H, ArH), 7.68-7.64 (m, 2H, ArH), 7.59 (br s, 1H, NH, exchangeable with D_2O), 7.44-7.41 (m, 1H, ArH), 7.33-7.14 (m, 4H, ArH), 6.91 (d, J = 2.1 Hz, 1H, ArH), 6.87 (d, J = 2.1 Hz, 1H, ArH), 3.74 (s, 3H, CH_3) ppm. ESI-MS (*m*/*z*) Calcd: 293 Found: 292 $[M-H]^-$. Anal. Calcd for $C_{18}H_{15}NO_3$: C, 73.71; H, 5.15; N, 4.78. Found: C, 73.59; H, 5.16; N, 4.76.

3-(4-Methoxy-1-naphthylamino)benzoic acid (7b). Procedure D: starting from **4b**. Reaction time: 60 min. Oil, 73 % yield. Molecular formula: $C_{18}H_{15}NO_3$. Molecular Weight: 293.32 g/mol. Rf = 0.16 (dichloromethane/methanol 95:5). ^{1}H NMR (300 MHz, $CO(CD_3)_2$) δ 11.00 (bs, 1H, OH, exchangeable with D_2O), 8.31–8.25 (m, 1H, ArH), 8.07 -7.99 (m, 1H, ArH), 7.55-7.45 (m, 3H, ArH), 7.42-7.36 (m, 2H, ArH), 7.34 (bs, 1H, NH, exchangeable with D_2O), 7.24 (t, J = 7.8 Hz, 1H, ArH), 7.00 (dd, J = 8.1, J_2 = 1.6 Hz, 1H, ArH), 6.96 (d, J = 8.2

Hz, 1H, ArH), 4.04 (s, 3H, CH_3) ppm. ESI-MS (*m*/*z*) Calcd: 293 Found: 292 $[M-H]^-$. Anal. Calcd for $C_{18}H_{15}NO_3$: C, 73.71; H, 5.15; N, 4.78. Found: C, 73.52; H, 5.14; N, 4.81.

2-(5-Methoxy-1-naphthylamino)benzoic acid (7c). Procedure D: starting from **4c**. Reaction time: 30 min. Solid, 203-205°C, 70% yield. Molecular formula: $C_{18}H_{15}NO_3$. Molecular Weight: 293.32 g/mol. Rf = 0.30 (dichloromethane/methanol 95:5). Eluent for chromatography: dichloromethane/methanol (95:5). ^{1}H NMR (300 MHz, CD_3OD) δ 7.98-7.95 (m, 1H, ArH), 7.64 (d, *J* = 8.4 Hz, 1H, ArH), 7.59 (s, 1H, ArH), 7.43 (d, *J* = 7.2 Hz, 1H, ArH), 7.38-7.33 (m, 3H, ArH), 7.25 (t, *J* = 7.7 Hz, 1H, ArH), 7.13 (d, *J* = 8.4 Hz, 1H, ArH), 6.92 (d, *J* = 7.7 Hz, 1H, ArH), 4.01 (s, 3H, CH_3).

3-((3-Hydroxynaphthalen-1-yl)amino)benzoic acid (7d). Procedure E: starting from **7a**. Reaction time: 210 minutes. Oil, 91 % yield. Molecular formula: $C_{17}H_{13}NO_3$. Molecular Weight: 279.29 g/mol. Rf = 0.17 (dichloromethane/methanol 95:5). ^{1}H NMR (300 MHz, $CO(CD_3)_2$) δ 7.93 (d, *J* = 8.0 Hz, 1H, ArH), 7.67 (s, 1H, ArH), 7.60-7.53 (m, 2H, ArH), 7.44-7.40 (m, 1H, ArH), 7.30-7.20 (m, 3H, ArH, NH, exchangeable with D_2O), 7.14-7.08 (m, 1H, ArH), 6.96 (d, *J* = 2.7 Hz, 1H, ArH), 6.81 (s, 1H, ArH) ppm. ESI-MS (*m*/*z*) Calcd: 279 Found: 278 $[M-H]^-$. Anal. Calcd for $C_{17}H_{13}NO_3$: C, 73.11; H, 4.69; N, 5.02. Found: C, 73.02; H, 4.70; N, 5.01.

3-(4-Hydroxy-1-naphthylamino)benzoic acid (7e). Procedure E: starting from **7b**. Reaction time: 60 min. Yellow oil, 89 % yield. Molecular formula: $C_{17}H_{13}NO_3$. Molecular Weight: 279.29 g/mol. Rf = 0.13 (dichloromethane/methanol 95:5). ^{1}H NMR (300 MHz, $CO(CD_3)_2$) δ 8.99 (br s, 1H, exchangeable with D_2O), 8.32-8.26 (m, 1H, ArH), 8.03-7.96 (m, 1H, ArH), 7.51-7.44 (m, 3H, ArH), 7.39-7.33 (m, 1H, ArH), 7.30-7.18 (m, 2H, ArH), 6.99-6.90 (m, 2H, ArH) ppm. ESI-MS (*m*/*z*) Calcd: 279 Found: 278 $[M-H]^-$. Anal. Calcd for $C_{17}H_{13}NO_3$: C, 73.11; H, 4.69; N, 5.02. Found: C, 73.13; H, 4.69; N, 5.02.

3-(5-Hydroxy-1-naphthylamino)benzoic acid (7f). Procedure E: starting from **7c**. Reaction time: 4 h. Yellow oil, 98% yield. Molecular formula: $C_{17}H_{13}NO_3$. Molecular Weight: 279.30 g/mol. Rf = 0.13 (dichloromethane/methanol 95:5). Eluent for chromatography: dichloromethane/methanol (95:5). ^{1}H NMR (300 MHz, $CO(CD_3)_2$) δ 9.14 (br s, 1H, NH exchangeable with D_2O), 8.03-8.00 (m, 1H, ArH), 7.72-7.62 (m, 2H, ArH, 1H, OH exchangeable with D_2O), 7.51-7.22 (m, 6H, ArH), 6.95 (dd, J_1 = 7.5 Hz, J_2 = 1.0 Hz, 1H, ArH). ESI-MS (*m*/*z*) Calcd: 279 Found: 278 $[M-H]^-$. Anal. Calcd for $C_{17}H_{13}NO_3$: C, 73.11; H, 4.69; N, 5.02. Found: C, 73.05; H, 4.68; N, 5.04.

3-(4-((*tert*-Butoxycarbonyl)amino)-1-naphthylamino)benzoic acid (7g). Procedure D: starting from **4g**. Reaction time: 30 min. Silver foam, quantative yield. Molecular formula: $C_{22}H_{22}N_2O_4$. Molecular Weight: 378.42 g/mol. Rf = 0.17 (dichloromethane/methanol 95:5). ^{1}H NMR (300 MHz, CD_3OD) δ 8.09 (d, *J* = 7.8 Hz, 1H, ArH), 8.01 (d, *J* = 8.7 Hz, 1H, ArH), 7.59-7.42 (m, 5H, ArH), 7.32 (d, *J* = 8.1 Hz, 1H, ArH), 7.24 (t, *J* = 7.8 Hz, 1H, ArH), 7.10-7.16 (m, 1H, ArH), 1.54 (s, 9H, CH_3) ppm.

3-(5-((*tert*-Butoxycarbonyl)amino)-1-naphthylamino)benzoic acid (7h). Procedure D: starting from **4h**. Reaction time: 30 min. Green-brown oil, 79 % yield. Molecular formula: $C_{22}H_{22}N_2O_4$. Molecular Weight: 378.42 g/mol. Rf = 0.20 (dichloromethane/methanol 95:5). ^{1}H NMR (300 MHz, $CO(CD_3)_2$) δ 8.19 (br s, 1H, NH, exchangeable with D_2O), 7.84 (d, *J* = 8.7 Hz, 1H, ArH), 7.75 (dd, J_1 = 6.9 Hz, J_2 = 3.0 Hz, 1H, ArH), 7.70 (d, *J* = 7.5 Hz, 1H, ArH), 7.58 (t, *J* = 2.1 Hz, 1H, ArH), 7.55 (br s, 1H, NH, exchangeable with D_2O), 7.40-7.28 (m, 4H, ArH), 7.20 (t, *J* = 7.5 Hz, 1H, ArH), 7.17-7.12 (m, 1H, ArH), 1.39 (s, 9H, CH_3) ppm.

3-(4-Amino-1-naphthylamino)benzoic acid hydrochloride (7i). Procedure F1: starting from **7g**. Foam, 58% yield. Molecular formula: $C_{17}H_{14}N_2O_2 \cdot HCl$. Molecular Weight: 314.77 g/mol. ^{1}H NMR (300 MHz, CD_3OD) δ 8.32 (d, *J* = 8.4 Hz, 1H, ArH), 7.93 (d, *J* = 8.4 Hz, 1H, ArH), 7.81-7.69 (m, 2H, ArH), 7.72-7.60 (m, 1H, ArH), 7.58 (d, *J* = 7.0 Hz, 1H, ArH), 7.47

(d, *J* = 8.4 Hz, 1H, ArH),7.41-7.24 (m, 3H, ArH) ppm. ESI-MS (*m*/*z*) Calcd: 278 Found: 277 $[M-H]^-$. Anal. Calcd for $C_{17}H_{15}ClN_2O_2$: C, 64.87; H, 4.80; Cl, 11.26. Found: C, 64.71; H, 4.82; Cl, 11.25.

3-(5-Amino-1-naphthylamino)benzoic acid hydrochloride (7j). Procedure F1: starting from **7h**. Foam, 66 % yield. Molecular formula: $C_{17}H_{14}N_2O_2 \cdot HCl$. Molecular Weight: 314.77 g/mol. ^1H NMR (300 MHz, CD_3OD) δ 8.28 (dd, J_1 = 8.1 Hz, J_2 = 1.2 Hz, 1H, ArH), 7.66 (t, *J* = 2.1 Hz, 1H, ArH), 7.63-7.49 (m, 6H, ArH), 7.34 (t, *J* = 7.8 Hz, 1H, ArH), 7. 28-7.24 (m, 1H, ArH) ppm. ESI-MS (*m*/*z*) Calcd: 278 Found: 277 $[M-H]^-$. Anal. Calcd for $C_{17}H_{15}ClN_2O_2$: C, 64.87; H, 4.80; Cl, 11.26. Found: C, 64.94; H, 4.81; Cl, 11.24.

Ethyl-2-(5-hydroxy-1-naphthylamino)benzoate (8). Procedure G: starting from **6f**. Green foam, 30% yield. Molecular formula: $C_{19}H_{17}NO_3$. Molecular Weight: 307.34 g/mol. Rf = 0.54 (cyclohexane/ethyl acetate 70:30). Eluent for chromatography: cyclohexane/ethyl acetate 70:30. ^1H NMR (300 MHz, $CDCl_3$) δ 9.80 (br s, 1H, NH exchangeable with D_2O), 8.1-8.0 (m, 2H, ArH), 7.68 (d, *J* = 8.6 Hz, 1H, ArH), 7.54 (d, *J* = 7.3 Hz, 1H, ArH), 7.46 (*t, J* = 7.8 Hz, 1H, ArH), 7.33-7.22 (m, 2H, ArH), 6.96 (d, *J* = 8.6 Hz, 1H, ArH), 6.85 (d, *J* = 7.4 Hz, 1H, ArH), 6.72 (t, *J* = 7.6 Hz, 1H, ArH), 4.40 (q, *J* = 7.1 Hz, 2H, CH_2), 1.44 (t, *J* = 7.1 Hz, 3H, CH_3), 1.25 (br s, 1H, OH exchangeable with D_2O). ESI-MS (*m*/*z*) Calcd: 307 Found: 306 $[M-H]^-$. Anal. Calcd for $C_{19}H_{17}NO_3$: C, 74.25; H, 5.58; N, 4.56. Found: C, 74.29; H, 5.56; N, 4.54.

Ethyl-3-(5-hydroxy-1-naphthylamino)benzoate (9). Procedure G: starting from **7f**. Yellow foam, 41% yield. Molecular formula: $C_{19}H_{17}NO_3$. Molecular Weight: 307.34 g/mol. Rf = 0.51 (cyclohexane/ethyl acetate 70:30). Eluent for chromatography: cyclohexane/ethyl acetate 70:30. ^1H NMR (300 MHz,$CDCl_3$) δ 8.64 (br s, 1H, NH exchangeable with D_2O), 8.15-8.05 (m, 1H, ArH), 7.85-7.70 (m, 2H, ArH), 7.64-7.50 (m, 2H, ArH), 7.46-7.40 (m, 2H, ArH), 7.38-7.30 (m, 2H, ArH), 7.15 (t, *J* = 7.1 Hz, 1H, ArH), 6.02 (br s, 1H, OH

exchangeable with D_2O), 4.10 (q, *J* = 7.0 Hz, 2H, CH_2), 1.40 (t, *J* = 7.0 Hz, 3H, CH_3). ESI-MS (*m*/*z*) Calcd: 307 Found: 306 $[M-H]^-$. Anal. Calcd for $C_{19}H_{17}NO_3$: C, 74.25; H, 5.58; N, 4.56. Found: C, 74.09; H, 5.61; N, 4.55.

Ethyl 2-(5-amino-1-naphthyamino)benzoate hydrochloride (10). Procedure F2: starting from **3h**. Green solid, 71.6% yield. Molecular formula: $C_{19}H_{18}N_2O_2 \cdot HCl$. Molecular Weight: 342.82 g/mol. Rf = 0.22 (cyclohexane/ethyl acetate 80:20). ^{1}H NMR (300 MHz, CD_3OD) δ 8.15-8.21 (m, 1H, ArH), 8.04 (dd, J_1=8.0 Hz, J_2=1.6 Hz, 1H, ArH), 7.65-7.83 (m, 3H, ArH), 7.55-7.61 (m, 2H, ArH), 7.25-7.37 (m, 1H, ArH), 7.00 (dd, J_1=8.5 Hz, J_2=0.8 Hz, 1H, ArH), 6.77-6.86 (m, 1H, ArH), 4.42 (q, *J*=7.1 Hz, 2H, CH_2), 1.43 (t, *J*=7.1 Hz, 3H, CH_3). ^{13}C-NMR (CD_3OD) δ 169.01, 148.09, 137.64, 134.06, 131.31, 129.94, 128.68, 128.04, 127.49, 125.41, 122.84, 120.49, 120.02, 117.60, 116.80, 114.13, 112.31, 60.81, 13.26. ESI-MS (*m*/*z*) Calcd: 306 Found: 305 $[M-H]^-$. Anal. Calcd for $C_{19}H_{19}ClN_2O_2$: C, 66.57; H, 5.59; Cl, 10.34; N, 8.17. Found: C, 66.69; H, 5.58; Cl, 10.43; N, 8.19.

Ethyl 3-(5-amino-1-naphthylamino)benzoate hydrochloride (11). Procedure F2: starting from **7j**. Blue solid, 86.4% yield. Molecular formula: $C_{19}H_{18}N_2O_2 \cdot HCl$. Molecular Weight: 342.82 g/mol. Rf = 0.17 (cyclohexane/ethyl acetate 80:20). ^{1}H NMR (300 MHz, CD_3OD) δ 8.28 (d, *J* = 8.1 Hz, 1H, ArH), 7.67-7.46 (m, 7H, ArH), 7.37-7.21 (m, 2H, ArH), 4.32 (q, *J* = 7.1 Hz, 2H, CH_2), 1.35 (t, *J*=7.1 Hz, 3H, CH_3). ^{13}C-NMR (CD_3OD) δ 166.79, 145.26, 140.44, 131.23, 128.98, 128.51, 128.00, 127.78, 127.47, 124.27, 123.70, 121.59, 120.85, 120.32, 117.63, 116.15, 114.24, 60.67, 13.14. ESI-MS (*m*/*z*) Calcd: 306 Found: 305 $[M-H]^-$. Anal. Calcd for $C_{19}H_{19}ClN_2O_2$: C, 66.57; H, 5.59; Cl, 10.34; N, 8.17. Found: C, 66.40; H, 5.58; Cl, 10.38; N, 8.13.

2-((5-Aminonaphthalen-1-yl)amino)benzoic acid hydrochloride (12). Procedure D: starting from **10**. Reaction time: 30 min. Grey solid, 48% yield. Molecular formula: $C_{17}H_{14}N_2O_2 \cdot HCl$. Molecular Weight: 314.77 g/mol. Rf = 0.26 (dichloromethane/methanol

95:5). Eluent for chromatography: dichloromethane/methanol (95:5). ^{1}H NMR (300 MHz, $(CD_3)_2SO$) δ 10.03 (br s, 1H, NH, exchangeable with D_2O), 8.00-7.76 (m, 3H, ArH), 7.68-7.42 (m, 4H, ArH), 7.31 (t, *J* = 7.8 Hz, 1H, ArH), 6.90 (d, *J*=8.4 Hz, 1H, ArH), 6.77 (t, *J* = 7.5 Hz, 1H, ArH), 3.65 (br s, 2H, NH_2, exchangeable with D_2O hidden under water peak) ^{13}C-NMR $(CD_3)_2SO$) δ 170.73, 148.64, 137.14, 134.72, 132.24, 129.85, 127.58, 126.89, 126.90, 126.60, 120.65, 118.98, 118.99, 117.87, 117.88, 114.42, 112.85. ESI-MS (*m*/*z*) Calcd: 278 Found: 277 $[M-H]^-$. Anal. Calcd for $C_{17}H_{14}N_2O_2$: C, 73.37; H, 5.07; N, 10.07. Found: C, 73.48; H, 5.09; N, 10.09.

Synthesis of 1-amino-2,4-dibromonaphthalene (13). To a solution of 1-aminonaphthalene (**24**) (250 mg, 1.745 mmol) in acetic acid (1 mL) was added a 0-5°C solution of Br_2 (0.27 mL, 5.235 mmol) in acetic acid (2 mL). Another 1 mL of acetic acid was added and the mixture was warmed at 60°C for 15 min, during which the color solution changed from purple to orange. Then, the mixture was cooled, and the salt was filtered, washed with acetic acid, and suspended in an excess of 1M NaOH. The product was collected by filtration, washed with water and dried to give a purple solid. The crude residue was purified by flash chromatography (cyclohexane/ethyl acetate 90:10) to provide compound **13**.[47] Violet solid m.p. 114-116°C, 86 % yield. Molecular formula: $C_{10}H_7Br_2N$. Molecular Weight: 300.98 g/mol. Rf = 0.33 (cyclohexane/ethyl acetate 8:2). ^{1}H NMR (300 MHz, $CDCl_3$) δ 8.20-8.17 (m, 1H, ArH) 7.8-7.76 (m, 2H, ArH), 7.62-7.50 (m, 2H, ArH), 4.63 (br s, 2H, NH_2, exchangeable with D_2O).

Synthesis of 4-bromo-2-hydroxynaphthalene-1-diazonium salt (14). To a stirred solution of compound **13** (250 mg, 0.831 mmol) in acetic acid (4 mL) and propionic acid (0.67 mL) at 8-10°C was gradually added sodium nitrite (86 mg, 1.246 mmol). After stirring for 10 min the yellow-brown solution was poured into 6 mL of ice water and the resulting mixture was rapidly filtered to remove a black tar. The aqueous phase was extracted with

dichloromethane (6×2 mL). The collected organic phase was dried over anhydrous sodium sulfate, filtered and the solvent was evaporated under *vacuum* to give compound **14**.[47] Yellow-orange solid (melting point: 118-125°C), 98 % yield. Molecular formula: $C_{10}H_6BrN_2O^+$. Molecular Weight: 250.96 g/mol. ^{1}H NMR (300 MHz, $CDCl_3$) δ 8.08 (d, J = 9 Hz, 1H, ArH), 7.58 (t, J = 9 Hz, 1H, ArH), 7.37 (t, J = 9 Hz, 1H, ArH), 7.28 (d, J = 9 Hz, 1H, ArH), 7.18 (s, 1H, ArH) ppm.

Synthesis of 4-bromonaphthalen-2-ol (**15a).** To a suspension of compound **14** (200 mg, 0.803 mmol) in ethanol (3.5 mL), $NaBH_4$ (30.4 mg, 0.803 mmol) was added at 0-10°C. The solution was stirred until gas evolution ceased and the mixture appeared darker. After evaporating ethanol, the remaining residue was poured into water, basified with 10% NaOH and then extracted with dichloromethane (2×2 mL), in order to purify the reaction mixture from the unreacted materials and impurities. Then, the collected alkaline aqueous solution, which contained the sodium salt of compound **15a**, was acidified with 3M HCl and extracted with ethyl acetate (2×2 mL). The organic layer was dried over anhydrous sodium sulfate and evaporated under reduced pressure, to afford a crude brown solid. The residue was purified by flash chromatography (cyclohexane/ethyl acetate 90:10 - Rf = 0.18) to provide the intermediate **15a**. Brown solid m.p. 118-119°C, 75 % yield. Molecular formula: $C_{10}H_7BrO$. Molecular Weight: 223.06 g/mol. ^{1}H NMR (300 MHz, $CDCl_3$) δ 8.14 (d, J = 7.8 Hz, 1H, ArH), 7.67 (d, J_1 = 6.9 Hz, J_2 = 1.8 Hz, 1H, ArH), 7.41-7.50 (m, 3H, ArH), 7.14 (d, J = 1.8 Hz, 1H, ArH), 4.98 (s, 1H, OH, exchangeable with D_2O) ppm.

1-Bromo-3-methoxynaphthalene (16a). Procedure H: starting from **15a**. Brown solid, m.p. 67-68°C, 97 % yield. Molecular formula: $C_{11}H_9BrO$. Molecular Weight: 237.09 g/mol. Rf = 0.66 (cyclohexane/ethyl acetate 90:10). ^{1}H NMR (300 MHz, $CDCl_3$) δ 8.15 (d, J = 7.5 Hz, 1H, ArH), 7.72 (d, J = 7.5 Hz, 1H, ArH), 7.52-7.41 (m, 3H, ArH), 7.12 (d, J = 2.4 Hz, 1H, ArH), 3.91 (s, 3H, CH_3) ppm.

1-Bromo-4-methoxynaphthalene (16b). Procedure H: starting from 4-bromonaphthalen-1-ol. Brown solid, m.p. 64-66°C, 98% yield. Molecular formula: $C_{11}H_9BrO$. Molecular Weight: 237.09 g/mol. Rf = 0.56 (cyclohexane/ethyl acetate 90:10). ^{1}H NMR (300 MHz, $CDCl_3$) δ 8.28 (d, *J* = 8.4 Hz, 1H, ArH), 8.18 (d, *J* = 8.4 Hz, 1H, ArH), 7.67-7.50 (m, 3H, ArH), 6.67 (d, *J* = 8.4 Hz, 1H, ArH), 3.98 (s, 3H, CH_3) ppm.

3-Methoxy-1-naphthaldehyde (17a). Procedure I: starting from **16a**. Yellow-brown solid, m.p. 59-61°C, 56% yield. Molecular formula: $C_{12}H_{10}O_2$. Molecular Weight: 186.21 g/mol. Rf = 0.38 (cyclohexane/ethyl acetate 90:10). ^{1}H NMR (300 MHz, $CDCl_3$) δ 10.36 (s, 1H, CHO), 9.16-9.02 (m, 1H, ArH), 7.84-7.75 (m, 1H, ArH), 7.68-7.60 (m, 1H, ArH), 7.57-7.47 (m, 2H, ArH), 7.38 (d, *J* = 2.5 Hz, 1H, ArH), 3.95 (s, 3H, CH_3) ppm.

4-Methoxy-1-naphthaldehyde (17b). Procedure I: starting from **16b**. Yellow-brown semi-solid, m.p. 34°C, 89 % yield. Molecular formula: $C_{12}H_{10}O_2$. Molecular Weight: 186.21 g/mol. Rf = 0.25 (cyclohexane/ethyl acetate 90:10). ^{1}H NMR (300 MHz, $CDCl_3$) δ 10.18 (s, 1H, CHO), 9.30 (d, *J* = 8.5 Hz, 1H, ArH), 8.32 (d, *J* = 8.5 Hz, 1H, ArH), 7.88 (d, *J* = 8.0 Hz, 1H, ArH), 7.69 (t, *J* = 7.9 Hz, 1H, ArH), 7.56 (t, *J* = 7.9 Hz, 1H, ArH), 6.88 (d, *J* = 8.0 Hz, 1H, ArH), 4.04 (s, 3H, OCH_3) ppm.

Synthesis of 4,4-dimethyl-2-(2-bromophenyl)oxazoline (19). Thionyl chloride (1.09 mL, 14.924 mmol) was added to 2-bromobenzoic acid (1000 mg, 4.975 mmol) under N_2 and the mixture was refluxed for 6 hours. Then, the excess of thionyl chloride was removed under *vacuum*. The ice-cold solution of the remaining acyl chloride in dry dichloromethane (2 mL) was added dropwise to a solution of 2-amino-2-methyl-1-propanol (886.9 mg, 9.950 mmol) in dichloromethane (2 mL) at 0°C. The mixture was stirred at room temperature for 2 hours. In order to purify the reaction mixture from the unreacted 2-amino-2-methyl-1-propanol, the organic phase was washed with 3N HCl (3×1 mL), dried over anhydrous sodium sulfate, filtered and the solvent was evaporated under reduced pressure. The crude **18** was used in the

following reaction without further purification. White foam, 98% yield. Molecular formula: $C_{11}H_{14}BrNO_2$. Molecular weight: 272.14 g/mol. Rf = 0.67 (dichloromethane/methanol 90:10). ^{1}H NMR (300 MHz, $CDCl_3$) δ 7.51 (dd, J_1 = 8.1 Hz, J_2 = 1.1 Hz, 1H, ArH), 7.43 (dd, J_1 = 7.7 Hz, J_2 = 1.8 Hz, 1H, ArH), 7.29 (dt, J_1 = 8.1 Hz, J_2 =1.1 Hz, 1H, ArH), 7.20 (dt, J_1 = 7.7 Hz, J_2 = 1.8 Hz, 1H, ArH), 5.97 (br s, 1H, exchangeable with D_2O), 3.96 (br s, 1H, exchangeable with D_2O), 3.63 (s, 2H, CH_2), 1.35 (s, 6H, CH_3) ppm.

Subsequently, thionyl chloride (1.07 mL, 14.625 mmol) was added dropwise to the benzamide **18** (1326.8 mg, 4.875 mmol). When the vigorous reaction subsided, 6 mL of dry diethyl ether was added to the yellow solution. After 6 hours, the excess of thionyl chloride was evaporated under reduced pressure to provide white crystals of the hydrochloride salt, which was neutralized with cold 20% sodium hydroxide (2 mL) and extracted with diethyl ether (3×2 mL). The organic phase was dried over anhydrous sodium sulfate and the solvent was evaporated under reduced pressure. The crude brown oil was purified by flash chromatography eluting firstly with cyclohexane/ethyl acetate (98:2) and then with cyclohexane/ethyl acetate (9:1) to afford intermediate **19**. Pale yellow solid, m.p. 36-38°C, 79 % yield. Molecular formula: $C_{11}H_{12}BrNO$. Molecular weight: 254.12 g/mol. Rf = 0.15 (cyclohexane / ethyl acetate 90:10). ^{1}H NMR (300 MHz, $CDCl_3$) δ 8.02 (s, 1H, ArH), 7.79 (d, J_1 = 8.1 Hz, 1H, ArH), 7.56 (d, J = 8.1 Hz, 1H, ArH), 7.19 (t, J_1 = 8.1 Hz, 1H, ArH), 4.05 (s, 2H, CH_2), 1.35 (s, 6H, CH_3).

3-(3-Methoxynaphthalen-1-yl)isobenzofuran-1(3*H*)-one (21a). Procedure J: starting from **17a**. Foam, 52 % yield. Molecular formula: $C_{19}H_{14}O_3$. Molecular Weight: 290.31 g/mol. Rf = 0.37 (cyclohexane/ethyl acetate 80:20). ^{1}H NMR (300 MHz, $CDCl_3$) δ 8.15 (d, J = 8.0 Hz, 1H, ArH), 7.97 (d, J = 8.0 Hz, 1H, ArH), 7.78 (d, J = 7.7 Hz, 1H, ArH), 7.60-7.37 (m, 5H, ArH), 7.17-7.06 (m, 2H, ArH), 6.86 (d, J = 2.5 Hz, 1H, ArH), 3.79 (s, 3H, CH_3) ppm.

3-(4-Methoxynaphthalen-1-yl)isobenzofuran-1(3*H*)-one (21b). Procedure J: starting from **17b**. White solid, m.p. 194-197°C, 21 % yield. Molecular formula: $C_{19}H_{14}O_3$. Molecular Weight: 290.31 g/mol. Rf = 0.41 (cyclohexane/ethyl acetate 80:20). ^{1}H NMR (300 MHz, $CDCl_3$) δ 8.29 (d, *J* = 8.1 Hz, 1H, ArH), 8.09 (d, *J* = 8.4 Hz, 1H, ArH), 7.94 (d, *J* = 7.2 Hz, 1H, ArH), 7.62-7.46 (m, 4H, ArH), 7.36 (d, *J* = 7.8 Hz, 1H, ArH), 7.09-7.06 (m, 2H, ArH), 6.63 (d, *J* = 8.1 Hz, 1H, ArH), 3.91 (s, 3H, CH_3) ppm.

Ethyl-2-bromobenzoate (22). Procedure B: starting compound: 2-bromobenzoic acid. Pail brown oil, 56 % yield. Molecular formula: $C_9H_9BrO_2$. Molecular Weight: 229.07 g/mol. Rf = 0.63 (cyclohexane/ethyl acetate 90:10). ^{1}H NMR (300 MHz, $CDCl_3$) δ 7.73 (dd, J_1 = 7.6 Hz, J_2 = 2 .0 Hz, 1H, ArH), 7.60 (dd, J_1 = 7.6 Hz, J_2 = 2.0 Hz, 1H, ArH), 7.28 (m, 2H, ArH), 4.36 (q, *J* = 7.2 Hz, 2H, CH_2), 1.36 (t, *J* = 7.2 Hz, 3H, CH_3) ppm.

Ethyl-3-bromobenzoate (23). Procedure B: starting compound: 3-bromobenzoic acid. Pail brown oil, 65% yield. Molecular formula: $C_9H_9BrO_2$. Molecular Weight: 229.07 g/mol. Rf = 0.72 (cyclohexane/ethyl acetate 90:10). ^{1}H NMR (300 MHz, $CDCl_3$) δ 8.18 (t, *J* = 1.2 Hz, 1H, ArH), 7.97 (dd, J_1 = 8.1 Hz, J_2 = 1.2 Hz, 1H, ArH), 7.67 (dd, J_1 = 8.1 Hz, J_2 = 1.2 Hz, 1H, ArH), 7.30 (t, *J* = 8.1 Hz, 1H, ArH), 4.37 (q, *J* = 7.2 Hz, 2H, CH_2), 1.39 (t, *J* = 7.2 Hz, 3H, CH_3) ppm.

1-Aminonaphthalene (24). Procedure K: starting from 1-nitronaphthalene. Reaction time: 10 min. Purple solid m.p. 47-50°C, 74 % yield. Molecular formula: $C_{10}H_9N$. Molecular Weight: 143.19 g/mol. Rf = 0.47 (cyclohexane/ethyl acetate 70:30). The product was purified by flash chromatography, eluting with cyclohexane/ethyl acetate from (80:20) to (70:30). ^{1}H NMR (300 MHz, $CDCl_3$) δ 8.00-7.80 (m, 2H, ArH), 7.60-7.40 (m, 2H, ArH), 6.82 (d, *J* = 6 Hz, 1H, ArH), 4.10 (br s, 2H, NH_2, exchangeable with D_2O) ppm.

1-Amino-4-methoxynaphthalene (25). Procedure K: starting from 1-methoxy-4-nitronaphthalene. Reaction time: 60 min. Light tan solid m.p. 38-40°C, 49 % yield. Molecular

formula: $C_{11}H_{11}NO$. Molecular Weight: 173.21 g/mol. Rf = 0.43 (cyclohexane/ethyl acetate 80:20). The product was used in the next reaction without any further purification. ^{1}H NMR (300 MHz, $CDCl_3$) δ 8.49-8.42 (m, 1H, ArH), 7.85-7.80 (m, 1H, ArH), 7.57-7.50 (m, 2H, ArH), 6.70-6.65 (m, 2H, ArH), 3.98 (s, 3H, CH_3), 3.80 (br s, 2H, NH_2, exchangeable with D_2O) ppm.

***tert*-Butyl (4-bromonaphthalen-1-yl)carbamate (26).** Procedure L: starting from 1-amino-4-bromonaphthalene. White Solid, m.p. 138-140°C, 98 % yield. Molecular formula: $C_{15}H_{16}BrNO_2$. Molecular Weight: 322.20 g/mol. Rf = 0.33 (cyclohexane/ethyl acetate 90:10). ^{1}H NMR (300 MHz, $CDCl_3$) δ 8.25 (d, *J* = 8.1 Hz, 1H, ArH), 7.86 (d, *J* = 8.0 Hz, 1H, ArH), 7.77-7.71 (m, 2H, ArH), 7.62-7.51 (m, 2H, ArH), 6.89 (br s, 1H, NH, exchangeable with D_2O), 1.56 (s, 9H, CH_3) ppm.

***tert*-Butyl (5-bromonaphthalen-1-yl)carbamate (27).** Procedure L: starting from 1-amino-5-bromonaphthalene. Light pink foam, 85 % yield. Molecular formula: $C_{15}H_{16}BrNO_2$. Molecular Weight: 322.20 g/mol. Rf = 0.53 (cyclohexane/ethyl acetate 80:20). ^{1}H NMR (300 MHz, $CDCl_3$) δ 8.06 (d, *J* = 8.7 Hz, 1H, ArH), 7.98-7.84 (m, 2H, ArH), 7.80 (d, *J* = 7.5 Hz, 1H, ArH), 7.57 (t, *J* = 8.1 Hz, 1H, ArH), 7.35 (t, *J* = 8.1 Hz, 1H, ArH), 6.78 (br s, 1H, NH, exchangeable with D_2O), 1.55 (s, 9H, CH_3) ppm.

Biological Methods.

Materials and Reagents. Stock solutions of the active compounds were prepared in dimethylsulfoxide (DMSO) at 20 mM concentration; when diluted in the aqueous solution, the final concentration of the various compounds never exceeded 50 μM. For the production of the recombinant forms of CDC25A, -B and -C catalytic domain, a heterologous expression system was used, constituted by the vectors pET28a-CDC25A-cd, pET28a-CDC25B-cd or pET28a-CDC25C-cd kindly provided by H. Bhattacharjee (Florida International University,

Herbert Wertheim College of Medicine, Miami, Florida) and the *Escherichia coli* BL21(DE3) strain from Novagen. In the preparation of the recombinant enzyme,[70] the buffers used for the purification procedure and storage were slightly modified by thoroughly replacing 10 mM β-mercaptoethanol as a reducing agent with 0.5 mM Tris-(2-carboxyethyl)-phosphine hydrochloride (TCEP). The phosphate-buffered saline (PBS) contained 10 mM Na_2HPO_4, 2 mM KH_2PO_4, pH 7.4, supplemented with 137 mM NaCl and 2.7 mM KCl. Dulbecco's modified Eagle's medium (DMEM), fetal bovine serum (FBS), L-glutamine, penicillin G, streptomycin and trypsin were purchased from Lonza (Milano, Italy). OMFP, propidium iodide (PI), crystal violet, and all other chemicals of analytical grade were purchased from Sigma. Rabbit polyclonal antibody against p-Cdk1 was purchased from Cell Signaling Technology (Boston, USA), whereas rabbit polyclonal antibody against β-actin, as well as HRP conjugated secondary antibody, were purchased from Santa Cruz Biotechnology (Heidelberg, Germany).

Kinetic Studies of the CDC25 Phosphatase Activity. A fluorimetric assay method was used to measure the dephosphorylation of OMFP catalyzed by the recombinant CDC25 forms, essentially as previously described.[27, 38] Briefly, the formation of the fluorescent product O-methylfluorescein was monitored continuously at 30°C, using a computer-assisted Cary Eclipse spectrofluorimeter (Varian) equipped with an electronic temperature controller. Excitation and emission wavelengths were set at 485 and 530 nm, respectively. Both excitation and emission slits were set at 10 nm. The 500-μL final volume of the reaction mixture, containing a fixed concentration of CDC25A, -B or -C ranging between 15 and 25 nM in 20 mM Tris-HCl, pH 7.8, 0.5 mM TCEP, was prepared in the absence or in the presence of various concentrations of each among thirty-one inhibitors. The reaction mixture also contained 1% (v/v) DMSO carried over from the inhibitors. After the addition of 0.5-25 μM OMFP, the velocity of OMFP hydrolysis (v_i) was measured and expressed as Arbitrary

Units per min (AU/min). The data of v_i were analyzed as a function of [OMFP] in double reciprocal Lineweaver-Burk plots, thus allowing the extrapolation of the maximum velocity of OMFP hydrolysis (V_{max}) and affinity for the substrate OMFP (K_M).

To measure the inhibition constant (K_i) of CDC25 forms towards the various compounds, the Lineweaver-Burk plot of phosphatase activity in the absence of inhibitor was compared with those obtained in the presence of different concentrations of inhibitor. The resulting values of K_M for OMFP and V_{max} in the presence of the inhibitor were then used to calculate the K_i according to the following equations. When the K_M remained essentially unchanged, but the V_{max} decreased after the addition of the inhibitor (non-competitive inhibition), the K_i was calculated with the equation: $K_i = V_{max+I} \bullet [I]/(V_{max} - V_{max+I})$, where V_{max+I} represents the V_{max} measured in the presence of the inhibitor (I). When both K_M and V_{max} underwent a similar and progressive decrease after the addition of the inhibitor (un-competitive inhibition), the K_i could be calculated with either the former equation or an alternate equation: $K_i = K_{M+I} \bullet [I]/(K_M - K_{M+I})$, where K_{M+I} represents the K_M measured in the presence of the inhibitor. On the other hand, in the case of mixed inhibition, only a rough evaluation of the K_i value was possible on the basis of the decrease of V_{max} and increase of K_M after the addition of the inhibitor.

Intrinsic Fluorescence Studies on CDC25B. Fluorescence spectra were recorded at 20°C, using a computer-assisted Cary Eclipse spectrofluorimeter (Varian) equipped with an electronic temperature controller. Unless otherwise indicated, the excitation wavelength was set at 280 nm; both excitation and emission slits were set at 10 nm. Briefly, a 500-µL final volume of a 1 µM solution of the recombinant CDC25B dissolved in 20 mM Tris•HCl, pH 7.8 buffer containing 0.5 mM TCEP and 0.5% (v/v) DMSO was directly prepared in a fluorimetric cuvette in the absence or in the presence of various NPA derivatives. Spectra

were recorded at a scan speed of 120 nm/min and corrected for the inner-filter effect due to the absorbance of the NPA derivatives at 280 nm.

Cell Cultures. The human melanoma cell lines A375 and A2058, deriving from a primary tumor or lymph nodal metastasis, respectively, were kindly provided from CEINGE (Naples, Italy). Cells were grown in DMEM supplemented with 10% FBS, 2 mM L-glutamine, 100 IU/mL penicillin G and 100 μg/mL streptomycin in humidified incubator at 37°C under 5% CO_2 atmosphere. The human skin fibroblast cell line BJ-5ta immortalized with the human telomerase reverse transcriptase (ref. Biochimie 95 (2013) 934-945) was cultured in a 4:1 mixture of DMEM and Medium 199 supplemented with 4 mM L-glutamine, 4.5 g/L glucose, 1.5 g/L sodium bicarbonate, 10% FBS, 100 IU/mL penicillin G, 100 mg/mL streptomycin and 0.01 mg/mL hygromycin B in humidified incubator at 37 C under 5% CO_2 atmosphere. All cells were split and seeded every three days, and used during their exponential phase of growth. Cell treatments were usually carried out after 24 h from plating.

MTT Assay. The 3-(4,5-dimethylthiazole-2-yl)-2,5-biphenyltetrazolium bromide (MTT) assay was used to detect cell viability essentially as previously described.[71] A2058 cells were plated in 96-well microtiter plates at 4×10^4 cells/well. After 24 h, cells were treated with different concentrations of the various inhibitors or with 0.5% (v/v) DMSO as a control vehicle. After 24, 48 or 72 h treatment and upon addition of 10 μL MTT solution in the dark, plates were incubated for 3 h at 37°C under 5% CO_2 atmosphere. After medium aspiration and solubilization of formazan crystals, the absorbance was measured at a wavelength of 570 nm using an ELISA plate reader (Bio-Rad, Milano, Italy).

Cell Cycle Analysis. Cells were seeded into 6-well plates at 3×10^5 cells/well for 24 h at 37°C; after the addition of 10 μM FP-21 or 0.5% (v/v) DMSO, the incubation of treated cells continued for 8 or 16 h. After each treatment, cells were harvested with trypsin, centrifuged and the pellet was resuspended in PBS. For cell cycle analysis, cells were fixed with 70%

(v/v) cold ethanol and stored at -20°C for 1 h. Then, cells were washed with cold PBS, centrifuged and the pellet was resuspended in 200 μL of a non-lysis solution containing 50 μg/mL PI. After incubation at 4°C for 30 min, cells were analyzed with a FACScan flow cytometer (Becton Dickinson) to evaluate the distribution of cell cycle phases.

Colony Formation Assay. Colony-forming assay was performed as previously described with some modifications.[72] Briefly, cells were seeded in duplicate in 6-well plates at a density of 4×10^2 cells per well. After 2/3-days, cells were treated with 0.5% (v/v) DMSO or different FP-21 concentrations and incubated for additional 10 days at 37°C. Then, colonies were stained with 1% (w/v) crystal violet in 50% (v/v) ethanol for 1 h at room temperature. Cells were photographed with a digital camera (Canon PowerShot G9); the number of colonies (≥ 50 cells per colony) was counted using ImageJ 1.42q software.

Total cell lysates and Western blotting. A2058 and A375 cells were seeded into 6-well-plates (3×10^5 cells/plate) for 24 h at 37 °C and then treated for 8 h with 10 μM compound **4a** or 0.5% DMSO. After treatment, cells were harvested, washed with PBS and then lysed in ice-cold modified radio immunoprecipitation assay (RIPA) buffer (50 mM Tris-HCl, pH 7.4, 150 mM NaCl, 1% Nonidet P-40, 0.25% sodium deoxycholate, 1 mM Na_3VO_4 and 1 mM NaF), supplemented with protease inhibitors and incubated for 30 min on ice. The supernatant obtained after centrifugation at 12,000 rpm for 30 min at 4°C constituted the total protein extract. Protein concentration was determined by the Bradford method, using bovine serum albumin (BSA) as standard.[73] Western blotting analysis was performed with equal amounts of total protein extracts. Briefly, protein samples were dissolved in SDS-reducing loading buffer, run on 12% SDS/PAGE and then transferred to Immobilon P membrane (Millipore). The filter was incubated with the specific primary antibody at 4°C overnight and then with the secondary antibody at room temperature for 1 h. Membranes were then

analyzed by an enhanced chemiluminescence reaction, using WesternBright ECL (Advansta) according to manufacturer's instruction; signals were visualized by autoradiography.

Statistical Analysis. Data are reported as the mean ± standard error (SE). The statistical significance of differences among groups was evaluated using ANOVA, with the Bonferroni correction as post hoc test or the Student *t* test where appropriate. The significance was accepted at the level of $p < 0.05$.

Molecular Modeling.

Ligand and Protein Preparation. The molecular structures of compounds **1-12** were sketched using the Molecular Builder module implemented in Maestro (Maestro, Schrödinger, LLC, New York, NY, 2018) and then preprocessed with LigPrep (LigPrep, Schrödinger, LLC, New York, NY, 2018). Multiple protonation and tautomerization states at pH of 7.0 +/- 2.0 were requested, although no additional ionization states were generated. The obtained structures were then energy-minimized by means of MacroModel 11.7 (MacroModel, Schrödinger, LLC, New York, NY, 2018) using the MMFF force field with the steepest descent (1000 steps) followed by truncated Newton conjugate gradient (500 steps) methods. Partial atomic charges were computed using the OPLS3 force field.[74]

Docking experiments were performed employing the crystal structure of the human Cdc25B catalytic domain (PDB ID: 1QB0).[22] This structure was selected because of its completeness, the absence of mutations, and the reasonably high resolution (1.9 Å). The protein setup was carried out using the Protein Preparation Wizard implemented in Maestro. Crystallographic water molecules and other chemical components were removed; hydrogen atoms were added to the protein consistent with the neutral physiologic pH. Arginine, lysine, aspartic and glutamic residues were considered ionized. Hydrogen bonds were optimized with PropKa (at pH 7.0), and a restrained minimization of the protein hydrogen atoms only

was conducted with the OPLS3 force field until an RMSD of 0.30 Å using the Impref module of Impact.

Docking Calculations. Since the receptor likely experiences conformational movements upon binding of ligands, docking simulations were performed with IFD module.[57, 58] Briefly, each ligand is first docked using a softened potential by means of Glide, which outputs a set of plausible poses. During this step, binding site residues are temporarily mutated to alanine, on the basis of the B-factors of the side chain atoms. A selected set of poses is then refined by Prime, which backmutates alanines to the original residues and performs a rotamer-based library optimization of the protein side chain conformations, to better accommodate the ligand. The best receptor structures are passed back to Glide for redocking of the ligand using the Glide XP scoring function. In this work, the docking grid was defined as the approximate center of the swimming pool, with an inner box size of 10 × 10 × 10 Å and an outer box of 30 × 30 × 30 Å.

With the aim to obtain a set of non-redundant poses and to save CPU time, the output poses from IFD simulations were clustered into separate self-organizing maps (SOMs) based on the Structural Interaction Fingerprints (SIFt)[75] contact similarity, as implemented in the Schrodinger Suite. The clusters were arranged in a 3 × 3 square matrix. Each cell in the cluster map contains a group of poses that are similar to one another in structural interaction fingerprint pattern. For each cluster, one representative was chosen for the subsequent binding pose metadynamics protocol. In this protocol, the selected poses underwent a series of metadynamics simulations by means of Desmond module, to determine the most stable one and provide a more reliable binding mode. The stability is assessed in terms of the fluctuations of the ligand RMSD over the course of the simulation, and the persistence of important contacts between the ligand and the receptor (and any other cofactors or solvent molecules), such as hydrogen bonds and π interactions. The collective variable for the

metadynamics simulation is the ligand RMSD from its initial pose. Since a biasing potential is applied to the ligand RMSD, an incorrect pose would easily be displaced than a more stable one. To improve the statistics, 10 metadynamics runs for each of the candidate poses were performed, and the results were averaged over the simulations. The poses were rank ordered by a Composite Score, linearly combining the average energy-weighted expectation of the pose RMSD over the course of metadynamics trajectories and the persistence of contacts between the protein and the ligand.

PAINS Filtering. All the tested compounds were screened for known classes of pan-assay interference compounds (PAINS)[76] by using Faf-Drugs4.[77] None of the compounds was found as potential PAINS. Furthermore, all the compounds were examined for known classes of molecular aggregators by using http://zinc15.docking.org/patterns/home/,[78] and none of them was found as a potential aggregator at the used final concentration. In addition, none of the compounds emitted fluorescence at the same wavelength as the substrate ligand OMFP in the fluorimetric assays.

Supporting Information

Kinetic parameters of the CDC25B phosphatase activity in the presence of compounds **1-12**, Lineweaver-Burk plots of non-competitive, un-competitive and mixed inhibitors, and structural analysis of Cdc25B crystal structures (PDF)

Molecular formula strings and the associated biological data (CSV)

Corresponding Author Information

Maria Rosaria Ruocco, Department of Molecular Medicine and Medical Biotechnology, University of Naples Federico II, 80131 Naples, Italy; Phone: +39-081-7463121; Fax: +39-081-7463653. E-mail: mariarosaria.ruocco2@unina.it

Antonio Lavecchia, Department of Pharmacy, "Drug Discovery" Laboratory, University of Naples Federico II, 80131 Naples, Italy; Phone: +39-081-678613/623; Fax: +39-081-678012. E-mail: antonio.lavecchia@unina.it

Author Contributions

[+]These authors contributed equally to this work

Acknowledgments

This study was supported by grants "Combattere la resistenza tumorale: piattaforma integrata multidisciplinare per un approccio tecnologico innovativo alle oncoterapie - CAMPANIA ONCOTERAPIE" (Project N. B61G18000470007) and "SATIN grant 2018-2020" of Regione Campania (Italy). The authors would like to thank Dr. Federica Porta, Marianna Porcino and Ilaria D'Andrea for their precious collaboration.

Abbreviations Used

BSA, bovine serum albumin; CDC25, cell division cycle 25; Cdk, cyclin-dependent kinases; DMEM, Dulbecco's modification of Eagle's medium; DMSO, dimethyl sulfoxide; DSP, dual-specificity phosphatase; FBS, foetal bovine serum; IFD, Induced Fit Docking; MTT, 3-[4,5-dimethylthiazol-2-yl]-2,5 diphenyl tetrazolium bromide; *n*-BuLi, *n*-Butyllithium; NPA, naphthylphenylamine; NPK, naphthylphenylketone; OMFP, 3-O-methyl fluorescein phosphate; PBS, phosphate-buffered saline; PDB, protein data bank; PI, propidium iodide; ROS, reactive oxygen species; SAR, structure-activity relationships; SDS/PAGE, sodium dodecyl sulfate polyacrylamide gel electrophoresis; SOMs, self-organizing maps; SIFt, Structural Interaction Fingerprints; TCEP, Tris-(2-carboxyethyl)-phosphine hydrochloride.

REFERENCES

1. Russell, P.; Nurse, P. cdc25+ functions as an inducer in the mitotic control of fission yeast. *Cell* **1986,** 45, 145-153.
2. Strausfeld, U.; Labbe, J. C.; Fesquet, D.; Cavadore, J. C.; Picard, A.; Sadhu, K.; Russell, P.; Doree, M. Dephosphorylation and activation of a p34cdc2/cyclin B complex in vitro by human CDC25 protein. *Nature* **1991,** 351, 242-245.
3. Aressy, B.; Bugler, B.; Valette, A.; Biard, D.; Ducommun, B. Moderate variations in CDC25B protein levels modulate the response to DNA damaging agents. *Cell Cycle* **2008,** 7, 2234-40.
4. Molinari, M.; Mercurio, C.; Dominguez, J.; Goubin, F.; Draetta, G. F. Human Cdc25 A inactivation in response to S phase inhibition and its role in preventing premature mitosis. *EMBO Rep* **2000,** 1, 71-9.
5. Karlsson-Rosenthal, C.; Millar, J. B. A. Cdc25: mechanisms of checkpoint inhibition and recovery. *Trends in Cell Biology* **2006,** 16, 285-292.
6. Terada, Y.; Tatsuka, M.; Jinno, S.; Okayama, H. Requirement for tyrosine phosphorylation of Cdk4 in Gl arrest induced by ultraviolet irradiation. *Nature* **1995,** 376, 358-362.
7. Massagué, J. Repression of the CDK activator Cdc25A and cell-cycle arrest by cytokine TGF-β in cells lacking the CDK inhibitor p15. *Nature* **1997,** 387, 417-422.
8. Lindqvist, A.; Rodríguez-Bravo, V.; Medema, R. H. The decision to enter mitosis: feedback and redundancy in the mitotic entry network. *The Journal of Cell Biology* **2009,** 185, 193-202.
9. Bartek, J.; Lukas, J. Mammalian G1- and S-phase checkpoints in response to DNA damage. *Current Opinion in Cell Biology* **2001,** 13, 738-747.
10. Boutros, R.; Lobjois, V.; Ducommun, B. CDC25 phosphatases in cancer cells: key players? Good targets? *Nat Rev Cancer* **2007,** 7, 495-507.
11. Fauman, E. B.; Saper, M. A. Structure and function of theprotein tyrosine phosphatases. *Trends Biochem. Sci* **1996,** 21, 413-417.
12. Gabrielli, B. G.; De Souza, C. P.; Tonks, I. D.; Clark, J. M.; Hayward, N. K.; Ellem, K. A. Cytoplasmic accumulation of cdc25B phosphatase in mitosis triggers centrosomal microtubule nucleation in HeLa cells. *J. Cell Sci.* **1996,** 109, 1081.
13. Izumi, T.; Maller, J. L. Phosphorylation and activation of the Xenopus Cdc25 phosphatase in the absence of Cdc2 and Cdk2 kinase activity. *Mol. Biol. Cell* **1995,** 6, 215-226.
14. Zwicker, J.; Lucibello, F. C.; Wolfraim, L. A.; Gross, C.; Truss, M.; Engeland, K.; Müller, R. Cell cycle regulation of the cyclin A, cdc25C and cdc2 genes is based on a common mechanism of transcriptional repression. *The EMBO Journal* **1995,** 14, 4514-4522.
15. Boutros, R.; Dozier, C.; Ducommun, B. The when and wheres of CDC25 phosphatases. *Curr. Opin. Cell Biol.* **2006,** 18, 185-191.
16. Liu, J. C.; Granieri, L.; Shrestha, M.; Wang, D.-Y.; Vorobieva, I.; Rubie, E. A.; Jones, R.; Ju, Y.; Pellecchia, G.; Jiang, Z. Identification of CDC25 as a Common Therapeutic Target for Triple-Negative Breast Cancer. *Cell reports* **2018,** 23, 112-126.
17. Hernández, S.; Bessa, X.; Beà, S.; Hernández, L.; Nadal, A.; Mallofré, C.; Muntane, J.; Castells, A.; Fernández, P. L.; Cardesa, A. Differential Expression of cdc25 Cell-Cycle–Activating Phosphatases in Human Colorectal Carcinoma. *Laboratory investigation* **2001,** 81, 465-473.
18. Wang, Z.; Trope, C. G.; Flørenes, V. A.; Suo, Z.; Nesland, J. M.; Holm, R. Overexpression of CDC25B, CDC25C and phospho-CDC25C (Ser216) in vulvar squamous cell carcinomas are associated with malignant features and aggressive cancer phenotypes. *BMC cancer* **2010,** 10, 233.
19. Kristjansdottir, K.; Rudolph, J. Cdc25 phosphatases and cancer. *Chemistry & biology* **2004,** 11, 1043-1051.
20. Albert, H.; Santos, S.; Battaglia, E.; Brito, M.; Monteiro, C.; Bagrel, D. Differential expression of CDC25 phosphatases splice variants in human breast cancer cells. *Clinical Chemistry and Laboratory Medicine* **2011,** 49, 1707-1714.

21. Fauman, E. B.; Cogswell, J. P.; Lovejoy, B.; Rocque, W. J.; Holmes, W.; Montana, V. G.; Piwnica-Worms, H.; Rink, M. J.; Saper, M. A. Crystal structure of the catalytic domain of the human cell cycle control phosphatase, Cdc25A. *Cell* **1998,** 93, 617-25.
22. Reynolds, R. A.; Yem, A. W.; Wolfe, C. L.; Deibel, M. R., Jr.; Chidester, C. G.; Watenpaugh, K. D. Crystal structure of the catalytic subunit of Cdc25B required for G2/M phase transition of the cell cycle. *J Mol Biol* **1999,** 293, 559-68.
23. Rudolph, J. Targeting the neighbor's pool. *Mol Pharmacol* **2004,** 66, 780-2.
24. Lavecchia, A.; Di Giovanni, C.; Novellino, E. CDC25 phosphatase inhibitors: an update. *Mini Rev. Med. Chem.* **2012,** 12, 62-73.
25. Lavecchia, A.; Coluccia, A.; Di Giovanni, C.; Novellino, E. Cdc25B phosphatase inhibitors in cancer therapy: latest developments, trends and medicinal chemistry perspective. *Anti-Cancer Agents in Medicinal Chemistry (Formerly Current Medicinal Chemistry-Anti-Cancer Agents)* **2008,** 8, 843-856.
26. Brenner, A. K.; Reikvam, H.; Lavecchia, A.; Bruserud, Ø. Therapeutic Targeting the Cell Division Cycle 25 (CDC25) Phosphatases in Human Acute Myeloid Leukemia—The Possibility to Target Several Kinases through Inhibition of the Various CDC25 Isoforms. *Molecules* **2014,** 19, 18414-18447.
27. Capasso, A.; Cerchia, C.; Di Giovanni, C.; Granato, G.; Albano, F.; Romano, S.; De Vendittis, E.; Ruocco, M. R.; Lavecchia, A. Ligand-based chemoinformatic discovery of a novel small molecule inhibitor targeting CDC25 dual specificity phosphatases and displaying in vitro efficacy against melanoma cells. *Oncotarget* **2015,** 6, 40202.
28. Kar, S.; Lefterov, I. M.; Wang, M.; Lazo, J. S.; Scott, C. N.; Wilcox, C. S.; Carr, B. I. Binding and inhibition of Cdc25 phosphatases by vitamin K analogues. *Biochemistry* **2003,** 42, 10490-7.
29. Pu, L.; Amoscato, A. A.; Bier, M. E.; Lazo, J. S. Dual G1 and G2 phase inhibition by a novel, selective Cdc25 inhibitor 6-chloro-7-[corrected](2-morpholin-4-ylethylamino)-quinoline-5,8-dione. *The Journal of biological chemistry* **2002,** 277, 46877-85.
30. Brisson, M.; Nguyen, T.; Wipf, P.; Joo, B.; Day, B. W.; Skoko, J. S.; Schreiber, E. M.; Foster, C.; Bansal, P.; Lazo, J. S. Redox regulation of Cdc25B by cell-active quinolinediones. *Molecular pharmacology* **2005,** 68, 1810-20.
31. Zhou, Y. B.; Feng, X.; Wang, L. N.; Du, J. Q.; Zhou, Y. Y.; Yu, H. P.; Zang, Y.; Li, J. Y.; Li, J. LGH00031, a novel ortho-quinonoid inhibitor of cell division cycle 25B, inhibits human cancer cells via ROS generation. *Acta pharmacologica Sinica* **2009,** 30, 1359-68.
32. Bolton, J. L.; Trush, M. A.; Penning, T. M.; Dryhurst, G.; Monks, T. J. Role of quinones in toxicology. *Chem Res Toxicol* **2000,** 13, 135-60.
33. Sohn, J.; Kiburz, B.; Li, Z.; Deng, L.; Safi, A.; Pirrung, M. C.; Rudolph, J. Inhibition of Cdc25 phosphatases by indolyldihydroxyquinones. *J Med Chem* **2003,** 46, 2580-8.
34. Brisson, M.; Nguyen, T.; Vogt, A.; Yalowich, J.; Giorgianni, A.; Tobi, D.; Bahar, I.; Stephenson, C. R.; Wipf, P.; Lazo, J. S. Discovery and characterization of novel small molecule inhibitors of human Cdc25B dual specificity phosphatase. *Molecular pharmacology* **2004,** 66, 824-33.
35. Kim, K. R.; Kwon, J. L.; Kim, J. S.; No, Z.; Kim, H. R.; Cheon, H. G. EK-6136 (3-methyl-4-(O-methyl-oximino)-1-phenylpyrazolin-5-one): a novel Cdc25B inhibitor with antiproliferative activity. *European journal of pharmacology* **2005,** 528, 37-42.
36. Kolb, S.; Mondesert, O.; Goddard, M. L.; Jullien, D.; Villoutreix, B. O.; Ducommun, B.; Garbay, C.; Braud, E. Development of novel thiazolopyrimidines as CDC25B phosphatase inhibitors. *ChemMedChem* **2009,** 4, 633-48.
37. George Rosenker, K. M.; Paquette, W. D.; Johnston, P. A.; Sharlow, E. R.; Vogt, A.; Bakan, A.; Lazo, J. S.; Wipf, P. Synthesis and biological evaluation of 3-aminoisoquinolin-1(2H)-one based inhibitors of the dual-specificity phosphatase Cdc25B. *Bioorganic & medicinal chemistry* **2015,** 23, 2810-8.

38. Lavecchia, A.; Di Giovanni, C.; Pesapane, A.; Montuori, N.; Ragno, P.; Martucci, N. M.; Masullo, M.; De Vendittis, E.; Novellino, E. Discovery of new inhibitors of Cdc25B dual specificity phosphatases by structure-based virtual screening. *J. Med. Chem.* **2012,** 55, 4142-4158.
39. Cerchia, C.; Lavecchia, A. Small Molecule Drugs and Targeted Therapy for Melanoma: Current Strategies and Future Directions. *Curr Med Chem* **2017,** 24, 2312-2344.
40. Bales, E. S.; Dietrich, C.; Bandyopadhyay, D.; Schwahn, D. J.; Xu, W.; Didenko, V.; Leiss, P.; Conrad, N.; Pereira-Smith, O.; Orengo, I. High levels of expression of p27KIP1 and cyclin E in invasive primary malignant melanomas. *J. Invest. Dermatol.* **1999,** 113, 1039-1046.
41. Tang, L.; Li, G.; Tron, V. A.; Trotter, M. J.; Ho, V. C. Expression of cell cycle regulators in human cutaneous malignant melanoma. *Melanoma Res.* **1999,** 9.
42. Muthusamy, V.; Hobbs, C.; Nogueira, C.; Cordon-Cardo, C.; McKee, P. H.; Chin, L.; Bosenberg, M. W. Amplification of CDK4 and MDM2 in malignant melanoma. *Genes, chromosomes & cancer* **2006,** 45, 447-54.
43. Lyons, J.; Bastian, B. C.; McCormick, F. MC1R and cAMP signaling inhibit cdc25B activity and delay cell cycle progression in melanoma cells. *Proc. Natl. Acad. Sci. U. S. A.* **2013,** 110, 13845-13850.
44. Yazdanian, M.; Glynn, S. L.; Wright, J. L.; Hawi, A. Correlating partitioning and caco-2 cell permeability of structurally diverse small molecular weight compounds. *Pharm Res* **1998,** 15, 1490-4.
45. Platt, K. L.; Oesch, F. Reductive cyclization of keto acids to polycyclic aromatic hydrocarbons by hydroiodic acid-red phosphorus. *The Journal of Organic Chemistry* **1981,** 46, 2601-2603.
46. Badger, G. M. Derivatives of o-1-naphthoylbenzoic acid and 1-benzylnaphthalene-2-carboxylic acid. *J. Chem. Soc* **1941**, 351-352.
47. Newman, M. S.; Sankaran, V.; Olson, D. R. Phenolic and ketonic tautomers in polycyclic aromatic hydrocarbons. *J. Am. Chem. Soc.* **1976,** 98, 3237-3242.
48. Harvey, R. G.; Cortez, C. Fluorine-substituted derivatives of the carcinogenic dihydrodiol and diol epoxide metabolites of 7-methyl-, 12-methyl-and 7, 12-dimethylbenz [a] anthracene. *Tetrahedron* **1997,** 53, 7101-7118.
49. Di Santo, R.; Costi, R.; Cuzzucoli Crucitti, G.; Pescatori, L.; Rosi, F.; Scipione, L.; Celona, D.; Vertechy, M.; Ghirardi, O.; Piovesan, P. Design, synthesis, and structure–activity relationship of N-arylnaphthylamine derivatives as amyloid aggregation inhibitors. *J. Med. Chem.* **2012,** 55, 8538-8548.
50. Vilaivan, T. A rate enhancement of tert-butoxycarbonylation of aromatic amines with Boc2O in alcoholic solvents. *Tetrahedron Lett.* **2006,** 47, 6739-6742.
51. Pini, E.; Poli, G.; Tuccinardi, T.; Chiarelli, L.; Mori, M.; Gelain, A.; Costantino, L.; Villa, S.; Meneghetti, F.; Barlocco, D. New Chromane-Based Derivatives as Inhibitors of Mycobacterium tuberculosis Salicylate Synthase (MbtI): Preliminary Biological Evaluation and Molecular Modeling Studies. *Molecules* **2018,** 23, 1506.
52. Chiarelli, L. R.; Mori, M.; Barlocco, D.; Beretta, G.; Gelain, A.; Pini, E.; Porcino, M.; Mori, G.; Stelitano, G.; Costantino, L.; Lapillo, M.; Bonanni, D.; Poli, G.; Tuccinardi, T.; Villa, S.; Meneghetti, F. Discovery and development of novel salicylate synthase (MbtI) furanic inhibitors as antitubercular agents. *Eur. J. Med. Chem.* **2018,** 155, 754-763.
53. Ge, Y.; van der Kamp, M.; Malaisree, M.; Liu, D.; Liu, Y.; Mulholland, A. J. Identification of the quinolinedione inhibitor binding site in Cdc25 phosphatase B through docking and molecular dynamics simulations. *J. Comput. Aided Mol. Des.* **2017,** 31, 995-1007.
54. Sarkis, M.; Miteva, M. A.; Dasso Lang, M. C.; Jaouen, M.; Sari, M. A.; Galcéra, M. O.; Ethève-Quelquejeu, M.; Garbay, C.; Bertho, G.; Braud, E. Insights into the interaction of high potency inhibitor IRC-083864 with phosphatase CDC25. *Proteins: Structure, Function, and Bioinformatics* **2017,** 85, 593-601.
55. Lazo, J. S.; Nemoto, K.; Pestell, K. E.; Cooley, K.; Southwick, E. C.; Mitchell, D. A.; Furey, W.; Gussio, R.; Zaharevitz, D. W.; Joo, B. Identification of a potent and selective pharmacophore for Cdc25 dual specificity phosphatase inhibitors. *Mol. Pharmacol.* **2002,** 61, 720-728.

56. Sohn, J.; Kristjánsdóttir, K.; Safi, A.; Parker, B.; Kiburz, B.; Rudolph, J. Remote hot spots mediate protein substrate recognition for the Cdc25 phosphatase. *Proc. Natl. Acad. Sci. U. S. A.* **2004,** 101, 16437-16441.
57. Sherman, W.; Day, T.; Jacobson, M. P.; Friesner, R. A.; Farid, R. Novel procedure for modeling ligand/receptor induced fit effects. *J. Med. Chem.* **2006,** 49, 534-553.
58. Sherman, W.; Beard, H. S.; Farid, R. Use of an induced fit receptor structure in virtual screening. *Chem. Biol. Drug Des.* **2006,** 67, 83-84.
59. Clark, A. J.; Tiwary, P.; Borrelli, K.; Feng, S.; Miller, E. B.; Abel, R.; Friesner, R. A.; Berne, B. J. Prediction of protein–ligand binding poses via a combination of induced fit docking and metadynamics simulations. *J. Chem. Theory Comput.* **2016,** 12, 2990-2998.
60. Sohn, J.; Kiburz, B.; Li, Z.; Deng, L.; Safi, A.; Pirrung, M. C.; Rudolph, J. Inhibition of Cdc25 phosphatases by indolylidihydroxyquinones. *J. Med. Chem.* **2003,** 46, 2580-2588.
61. Lavecchia, A.; Cosconati, S.; Limongelli, V.; Novellino, E. Modeling of Cdc25B dual specifity protein phosphatase inhibitors: Docking of ligands and enzymatic inhibition mechanism. *ChemMedChem: Chemistry Enabling Drug Discovery* **2006,** 1, 540-550.
62. Taylor, N. R.; Borhani, D.; Epstein, D.; Rudolph, J.; Ritter, K.; Fujimori, T.; Robinson, S.; Eckstein, J.; Haupt, A.; Walker, N.; Dixon, R. W.; Choquette, D.; Blanchard, J.; Kluge, A.; Pal, K.; Bockovich, N.; Come, J.; Hediger, M. Method of Identifying Inhibitors of Cdc25. WO0116300 (A2), 2001/03/08/, 2001.
63. Cheng, L.; Lopez-Beltran, A.; Massari, F.; MacLennan, G. T.; Montironi, R. Molecular testing for BRAF mutations to inform melanoma treatment decisions: a move toward precision medicine. *Mod. Pathol.* **2018,** 31, 24.
64. Franken, N. A. P.; Rodermond, H. M.; Stap, J.; Haveman, J.; Van Bree, C. Clonogenic assay of cells in vitro. *Nat. Protoc.* **2006,** 1, 2315.
65. Rudolph, J. Cdc25 phosphatases: structure, specificity, and mechanism. *Biochemistry* **2007,** 46, 3595-604.
66. Aressy, B.; Ducommun, B. Cell cycle control by the CDC25 phosphatases. *Anti-cancer agents in medicinal chemistry* **2008,** 8, 818-24.
67. Morgan, D. O. Principles of CDK regulation. *Nature* **1995,** 374, 131-4.
68. Hoffmann, I.; Clarke, P. R.; Marcote, M. J.; Karsenti, E.; Draetta, G. Phosphorylation and activation of human cdc25-C by cdc2--cyclin B and its involvement in the self-amplification of MPF at mitosis. *EMBO J* **1993,** 12, 53-63.
69. Yamaura, M.; Mitsushita, J.; Furuta, S.; Kiniwa, Y.; Ashida, A.; Goto, Y.; Shang, W. H.; Kubodera, M.; Kato, M.; Takata, M.; Saida, T.; Kamata, T. NADPH oxidase 4 contributes to transformation phenotype of melanoma cells by regulating G2-M cell cycle progression. *Cancer research* **2009,** 69, 2647-54.
70. Bhattacharjee, H.; Sheng, J.; Ajees, A. A.; Mukhopadhyay, R.; Rosen, B. P. Adventitious arsenate reductase activity of the catalytic domain of the human Cdc25B and Cdc25C phosphatases. *Biochemistry* **2010,** 49, 802-809.
71. Gelzo, M.; Granato, G.; Albano, F.; Arcucci, A.; Russo, A. D.; De Vendittis, E.; Ruocco, M. R.; Corso, G. Evaluation of cytotoxic effects of 7-dehydrocholesterol on melanoma cells. *Free Radical Biol. Med.* **2014,** 70, 129-140.
72. Rafehi, H.; Orlowski, C.; Georgiadis, G. T.; Ververis, K.; El-Osta, A.; Karagiannis, T. C. Clonogenic assay: adherent cells. *Journal of visualized experiments: JoVE* **2011**.
73. Bradford, M. M. A rapid and sensitive method for the quantitation of microgram quantities of protein utilizing the principle of protein-dye binding. *Analytical biochemistry* **1976,** 72, 248-54.
74. Harder, E.; Damm, W.; Maple, J.; Wu, C.; Reboul, M.; Xiang, J. Y.; Wang, L.; Lupyan, D.; Dahlgren, M. K.; Knight, J. L. OPLS3: a force field providing broad coverage of drug-like small molecules and proteins. *J. Chem. Theory Comput.* **2015,** 12, 281-296.
75. Deng, Z.; Chuaqui, C.; Singh, J. Structural interaction fingerprint (SIFt): a novel method for analyzing three-dimensional protein− ligand binding interactions. *J. Med. Chem.* **2004,** 47, 337-344.

76. Baell, J. B.; Holloway, G. A. New Substructure Filters for Removal of Pan Assay Interference Compounds (PAINS) from Screening Libraries and for Their Exclusion in Bioassays. *J. Med. Chem.* **2010,** 53, 2719-2740.
77. Lagorce, D.; Sperandio, O.; Baell, J. B.; Miteva, M. A.; Villoutreix, B. O. FAF-Drugs3: a web server for compound property calculation and chemical library design. *Nucleic Acids Res.* **2015,** 43, W200-W207.
78. Sterling, T.; Irwin, J. J. ZINC 15 – Ligand Discovery for Everyone. *J. Chem. Inf. Model.* **2015,** 55, 2324-2337.

FIGURE LEGENDS

Figure 1. Known reversible CDC25 Inhibitors.

Figure 2. Structure-based optimization of lead NSC28620. (A) Predicted binding mode of NSC28620 (green) in the CDC25B binding cavity. For clarity, only interacting residues are displayed and labeled. Ligand and interacting key residues (white) are represented as stick models, while the protein is a transparent Connolly surface model. H-bonds and salt bridges are shown as dashed black lines. (B) Schematic overview of the rationally designed NSC28620 derivatives.

Figure 3. Effect of compound **7j** or **3** on the Lineweaver-Burk plots of the CDC25B phosphatase activity. The activity, measured through the OMFP hydrolysis rate as described in the Experimental Section, was determined in the absence (open circles in both panels) or in the presence of 1.0 μM or 2.0 μM compound **7j** (filled triangles or filled circles, respectively; panel A) or 1.5 μM or 3.0 μM compound **3** (filled triangles or filled circles, respectively; panel B).

Figure 4. Effect of some NPA derivatives on the intrinsic fluorescence of CDC25B. The emission spectrum of 1 μM recombinant CDC25B in 20 mM Tris•HCl, pH 7.8 buffer containing 0.5 mM TCEP and 0.5% (v/v) DMSO was recorded at 20°C using the excitation wavelength of 280 nm, either in the absence (black line) or in the presence of 1.5 μM **7j**

(purple line), 3 μM **7i** (green line), 4 μM **3** (red line), or 10 μM **4a** (blue line).

Figure 5. (A) Binding mode of compound **7j** (green) into the swimming pool site of CDC25B (PDB ID: 1QB0). (B) Binding mode of compound **3** (cyan) to CDC25B in complex with the artificial OMFP substrate. For clarity, only interacting residues are displayed and labeled. Ligands and interacting key residues (white) are represented as stick models, while the protein is a slate ribbon model. The catalytic site and the adjacent deeper and larger swimming pool site are displayed as bluewhite Connolly surface. H-bonds and salt bridges are shown as dashed grey lines.

Figure 6. Cell toxicity of NPA derivatives. Panels A and B. A2058 cells were incubated for 48 or 72 h with 0.5 % (v/v) DMSO (open bars), 2.5 μM (gray bars) or 5.0 μM (black bars) of compound **4** (panel A) or **4a** (panel B). Panel C. BJ-5ta cells were incubated for 24, 48 or 72 h with 0.5 % (v/v) DMSO (open bars), 2.5 μM (light gray bars), 5.0 μM (dark gray bars) or 10 μM (black bars) of compound **4a**. Data of cell viability were obtained from at least three independent experiments and expressed in arbitrary units (AU), as the mean ± SE. **, $p < 0.01$; ***, $p < 0.001$ compared to control cells. Other details are in the Experimental Section.

Figure 7. Effect of **4a** on the colony formation of melanoma cells. A2058 and A375 cells were treated with vehicle alone or 0.625, 1.25, 2.5, 5.0, or 10 μM **4a**. After 10-days treatment, plates were photographed and images of representative experiments are shown. The bottom plots report the number of colonies counted as indicated in the Experimental Section; values are expressed in percentages and reported as the mean ± SE from at least three different experiments.

Figure 8. Effect of **4a** on the distribution of cell cycle phases of A2058 cells. The distribution of cells in the different phases was evaluated after 8 h (panels **A** and **C**) or 16 h (panels **B** and **D**) from treatment with 0.5% DMSO (Panels **A** and **B**) or 10 μM **4a** (Panels **C** and **D**) as described in the Experimental Section. Cell cycle phases colours: sub G1, light blue; G0/G1, red; S, green; G2/M, dark blue. Histograms show the cell percentage distribution among the various phases after 8 h (Panel **E**) or 16 h (Panel **F**). Data obtained from triplicate experiments in the presence of DMSO (open bars) or **4a** (black bars) are reported as the mean ± SE. ****, $p < 0.0001$ compared to control cells.

Figure 9. Effect of **4a** on the distribution of cell cycle phases of A375 cells. The same protocol described in the legend to Fig. 8 was followed for analyzing the cell phases distribution of A375 cells. **, $p < 0.01$; ****, $p < 0.0001$ compared to control cells.

Figure 10. Effect of **4a** on p-Cdk1 protein levels. A2058 and A375 cells were incubated in the absence or in the presence of 10 μM **4a** for 8 h and total protein extracts were used to detect p-Cdk1 levels through Western blot. β-actin was used as an internal loading control. *, $p < 0.05$ compared to control cells.

SCHEME LEGENDS

Scheme 1. Synthesis of 2-(1-naphthoyl)benzoic acid 1 and its ethyl ester 2.[a]

[a]Reagents and conditions: i) a. Mg, dry THF, N_2, reflux, 1h; b. phthalic anhydride, dry THF, N_2, reflux, 48 h; ii) EtOH, H_2SO_4, reflux, 24 h.

Scheme 2. Synthesis of 2-(3(4)-methoxy-1-naphthyl)benzoic acids 1a,b and 2-(3-hydroxy-1-naphthoyl)benzoic acid 1c.[a]

[a]Reagents and conditions: i) Br_2, AcOH, 60°C, 15 min; ii) $NaNO_2$, AcOH, 8-10°C, 10 min; iii) $NaBH_4$, EtOH, 0-10°C, 2-3 h; iv) a. NaH, dry DMF, N_2, rt, 15 min; b. CH_3I, dry DMF, N_2, rt, 3h; v) *n*-BuLi, dry THF, N_2, -78°C, 1 h; vi) dry DMF, dry THF, N_2, -78°C, 1 h; vii) a. $SOCl_2$, N_2, reflux, 6 h; b. 2-amino-2-methyl-1-propanol, dry DCM, N_2, rt, 2 h; viii) a. $SOCl_2$, N_2, rt, 30 min; b. dry Et_2O, 30 min; c. 20% NaOH; ix) *n*-BuLi, dry Et_2O, N_2, -78°C, 1 h; x) a. dry Et_2O, N_2, rt, overnight; b. 3M HCl, reflux, 4.5 h; c. 10% NaOH, reflux, 1 h; xi) 25% KOH, $KMnO_4$, Py, reflux, 5 h; xii) BBr_3 (1M in DCM), dry DCM, N_2, rt, 30-210 min.

Scheme 3. Synthesis of ethyl-(naphthylamino)benzoates 3, 3a-c, 3h, 4, 4a-c, 4g,h and 5.[a]

[a]Reagents and conditions: i) $Pd(OAc)_2$, (±)-BINAP, Cs_2CO_3, dry toluene, Ar, 80°C, 17-40 h.

Scheme 4. Synthesis of (naphthylamino)benzoic acid derivatives 6, 6a-f, 7, 7a-j, 8-12.[a]

[a]Reagents and conditions: i) 1M NaOH, THF/EtOH (1:1), reflux, 30-90 min; ii) a) HCl (4M in 1,4-dioxane), dry 1,4-dioxane, r.t., 24 h, or trifluoroacetic acid, dichloromethane, r.t., 60 min. (for **10** and **11**); b) BBr_3 (1M in dichloromethane), dry dichloromethane, N_2, r.t., 30-210 min; iii) H_2SO_4, EtOH, MW 80°C, 90 min (for **8** and **9**).

TABLES

Table 1. Rationally Designed Compounds **1-12** and their Inhibition Kinetic Parameters against CDC25B.

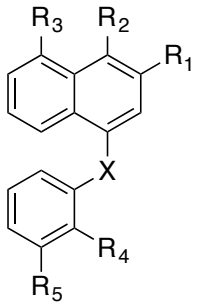

1-12

Cpd	R^1	R^2	R^3	R^4	R^5	X	K_i [a] (μM)	Putative inhibition mechanism
1	H	H	H	COOH	H	CO	69	mixed
1a	OCH_3	H	H	COOH	H	CO	36	mixed
1b	H	OCH_3	H	COOH	H	CO	7.1 ± 0.9	non-competitive
1c	OH	H	H	COOH	H	CO	34 ± 3	non-competitive
2	H	H	H	$COOC_2H_5$	H	CO	54	mixed
3	H	H	H	$COOC_2H_5$	H	NH	2.8 ± 0.7	un-competitive
3a	OCH_3	H	H	$COOC_2H_5$	H	NH	12.5 ± 2.6	un-competitive
3b	H	OCH_3	H	$COOC_2H_5$	H	NH	6.9 ± 2.0	non-competitive
4	H	H	H	H	$COOC_2H_5$	NH	7.3 ± 0.6	un-competitive
4a	OCH_3	H	H	H	$COOC_2H_5$	NH	8.5 ± 1.2	un-competitive
4b	H	OCH_3	H	H	$COOC_2H_5$	NH	11.9 ± 4.2	non-competitive
5	H	H	H	H	H	NH	32	mixed
6	H	H	H	COOH	H	NH	22 ± 3	un-competitive
6a	OCH_3	H	H	COOH	H	NH	16.9 ± 0.3	non-competitive
6b	H	OCH_3	H	COOH	H	NH	6.1 ± 0.7	un-competitive
6d	OH	H	H	COOH	H	NH	5.1 ± 0.7	non-competitive
6e	H	OH	H	COOH	H	NH	2.7 ± 1.1	non-competitive
6f	H	H	OH	COOH	H	NH	13.4 ± 1.1	non-competitive
7	H	H	H	H	COOH	NH	30	mixed
7a	OCH_3	H	H	H	COOH	NH	55 ± 7	un-competitive

7b	H	OCH_3	H	H	COOH	NH	45 ± 3	un-competitive
7d	OH	H	H	H	COOH	NH	5.8 ± 0.8	non-competitive
7e	H	OH	H	H	COOH	NH	6.4 ± 0.8	un-competitive
7f	H	H	OH	H	COOH	NH	2.9 ± 0.3	non-competitive
7i[b]	H	NH_2	H	H	COOH	NH	1.4 ± 0.3	non-competitive
7j[b]	H	H	NH_2	H	COOH	NH	0.8 ± 0.2	non-competitive
8	H	H	OH	$COOC_2H_5$	H	NH	7.4 ± 2.2	non-competitive
9	H	H	OH	H	$COOC_2H_5$	NH	4.9 ± 1.3	non-competitive
10[b]	H	H	NH_2	$COOC_2H_5$	H	NH	9.9 ± 3.2	non-competitive
11[b]	H	H	NH_2	H	$COOC_2H_5$	NH	36 ± 3	non-competitive
12	H	H	NH_2	COOH	H	NH	6.5 ± 1.4	non-competitive
NSC28620[38]							5.3 ± 2.4	competitive

[a] The values of K_i, calculated as indicated in the Experimental Section, are an average from at least three independent experiments. The missing standard deviation for mixed inhibitors is due to the fact that the K_i value indicated is just a rough evaluation of the inhibition power.
[b] Compounds were tested as hydrochloride salts.

Table of Contents graphic